Received: 19 July 2022 | Revised: 31 October 2022 | Accepted: 4 November 2022

DOI: 10.1002/cne.25435

RESEARCH ARTICLE

JCN RESEARCH IN SYSTEMS NEUROSCIENCE THE JOURNAL OF COMPARATIVE NEUROLOGY WILEY

Diversity of cellular physiology and morphology of Purkinje cells in the adult zebrafish cerebellum

Gerhard Magnus[1,2] | Junling Xing[3] | Yueping Zhang[2,3] | Victor Z. Han[1,2]

[1]Department of Biology, University of Washington, Seattle, Washington, USA

[2]Center for Integrative Brain Research, Seattle Children's Research Institute, Seattle, Washington, USA

[3]Department of Pediatrics and Neuroscience, Xijing Hospital, Xi'an, China

Correspondence
Gerhard Magnus, Department of Biology, University of Washington, Seattle, WA 98195, USA.
Email: magnusg1@uw.edu

Victor Z. Han, Department of Biology, University of Washington, Seattle, WA 98195, USA.
Email: vhan@uw.edu

Funding information
This work was supported by a grant from the National Science Foundation (IOS 1929489 to VZH), by the REP Program from Seattle Children's Research Institute (to VZH), and by a grand from China National Natural Science Foundation (to YZ)

Abstract

This study was designed to explore the functional circuitry of the adult zebrafish cerebellum, focusing on its Purkinje cells and using whole-cell patch recordings and single cell labeling in slice preparations. Following physiological characterizations, the recorded single cells were labeled for morphological identification. It was found that the zebrafish Purkinje cells are surprisingly diverse. Based on their physiology and morphology, they can be classified into at least three subtypes: Type I, a *narrow spike cell*, which fires only narrow Na^+ spikes (<3 ms in duration), and has a single primary dendrite with an arbor restricted to the distal molecular layer; Type II, a *broad spike cell*, which fires broad Ca^{2+} spikes (5–7 ms in duration) and has a primary dendrite with limited branching in the inner molecular layer and then further radiates throughout the molecular layer; and Type III, a *very broad spike cell*, which fires very broad Ca^{2+} spikes (≥10 ms in duration) and has a dense proximal dendritic arbor that is either restricted to the inner molecular layer (Type IIIa), or radiates throughout the entire molecular layer (Type IIIb). The graded paired-pulse facilitation of these Purkinje cells' responses to parallel fiber activations and the all-or-none, paired-pulse depression of climbing fiber activation are largely similar to those reported for mammals. The labeled axon terminals of these Purkinje cells end locally, as reported for larval zebrafish. The present study provides evidence that the corresponding functional circuitry and information processing differ from what has been well-established in the mammalian cerebellum.

KEYWORDS
adult zebrafish, cerebellum, climbing fiber, eurydendroid cells, parallel fiber, Purkinje cell morphology, Purkinje cell spikes

1 | INTRODUCTION

The mammalian cerebellum is a unique system consisting of numerous functional organizations or modules (Cerminara et al., 2015; Friedrich et al., 2010; Kalueff et al., 2014; Voogd & Glickstein, 1998). Each of these structures is believed to be similar, if not identical, in its local circuitry (Cerminara & Apps, 2011; Voogd & Glickstein, 1998). Thus, it is the external connectivity, not the inner computation, which determines each module's functionality and purpose. These cerebellar functions have been shown to extend over a wide range of applications, from motor control and learning to cognition and emotion (Buckner, 2013; Schmahmann et al., 2019).

The neuron of central importance in these cerebellar modules is the Purkinje cell. It is estimated that the human cerebellum contains roughly 15 million such Purkinje cells (Nairn et al., 1989), all of which share a similar morphology. A large soma emits a highly branched, fan-shaped dendritic tree, which is oriented in the parasagittal plane and is equipped with up to 180,000 dendritic spines, specialized

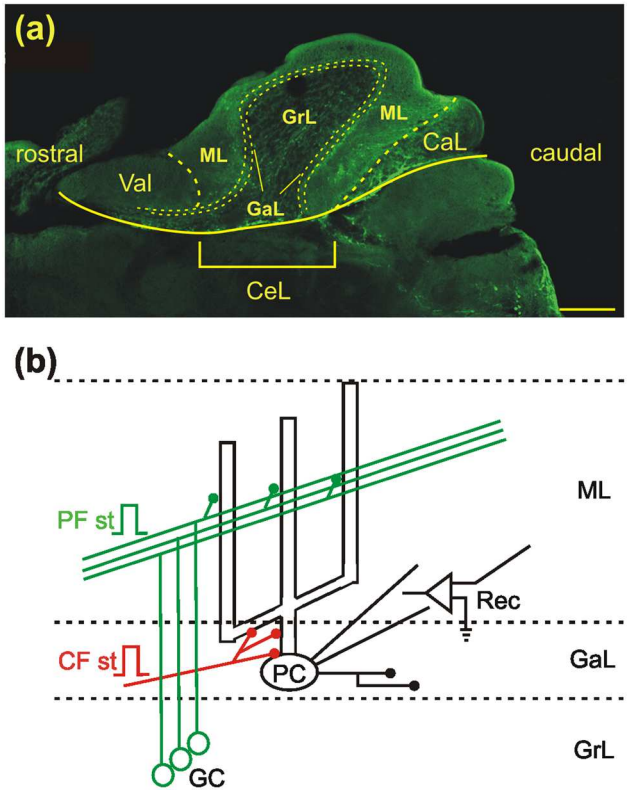

FIGURE 1 Experimental design. (a) Photomicrograph of an adult transgenic Tg(*Ptf1a-GFP*) zebrafish cerebellum in a parasagittal plane near the midline, showing expression of the vesicular glutamate transporter (green). Structures above the yellow line are the cerebellum (from rostral to caudal): valvula (Val), central lobe (CeL), and caudal lobe (CaL). The central lobe (between the thick dashed lines) occupies much of the cerebellum, and consists of three layers: the molecular layer (ML), ganglionic layer (GaL, between the thin dashed lines), and granular layer (GrL). This study focuses on Purkinje cells in the central lobe. Scale bar = 200 µm. (b) Experimental configuration. Whole-cell patch recordings (Rec) were carried out from the Purkinje cell soma, with stimulus electrodes positioned in the ML and GaL to activate PFs and a single CF, respectively.

postsynaptic structures that receive synaptic inputs (Ito, 1984). Purkinje cells receive two excitatory inputs, climbing fibers and parallel fibers (CFs and PFs; Figure 1b), where the former originate in the contralateral inferior olive and the latter are the axons of up to 50 billion granule cells (Azevedo et al., 2009; Herculano-Houzel, 2009). A single CF makes a few hundred synapses onto the soma and dendritic arbor of the Purkinje cell to which it projects (Eccles, 1967; Meek & Nieuwenhuys, 1991). The PFs run mediolaterally, perpendicular to the fan-shaped arrays of Purkinje cell dendrites, and parallel to each other (Meek & Nieuwenhuys, 1991). Hence, each PF makes synaptic contact with numerous Purkinje cells, but only a single synaptic contact with each one (Eccles, 1967). Purkinje cells then integrate these two excitatory input signals along with inhibition from inhibitory interneurons (Ito, 1984) and other Purkinje cells (Sugihara et al., 2009), and convey all their output information via collateralized axons to inhibit cells in the deep cerebellar nuclei (DCN) and vestibular nuclei (VN) (Sugihara & Shinoda, 2007). These, in turn, project to numerous targets outside the cerebellum (Ito, 1984; Gilbert & Thach, 1977). This modular circuitry has been established throughout vertebrates (Meek, 1998) and become the basic criterion for determining whether a central structure is to be considered cerebellar-like or not (Cerminara et al., 2015; Kalueff et al., 2014).

Over more than half a century, the mammalian cerebellum has been extensively studied, from investigations of the molecular biology of its cells (Ito, 2002) to clinical studies involving cerebellum-influenced behavior (Dow & Moruzzi, 1958; Ito, 2008), and at variety of physiological and network levels in between (Buckner, 2013; Schmahmann et al., 2019). In one much-studied instance connecting neuron electrophysiology to conditioned behavior, unconditional signals, such as air-puff to the eye or a minor electric shock, have been found to conduct along the CFs, whereas conditioning signals, such as a tone or flash of light, are relayed to the cerebellar cortex by the mossy fiber/PF system. These two types of input signals are integrated by Purkinje cells, which in turn send motor behavior-related signals to the DCN and VN (Linden, 2003). Our understanding of Purkinje cells is crucial to understand how the cerebellar cortex computes a variety of similarly relayed input signals and generates meaningful biological information (Cerminara et al, 2015; Lee et al., 2015). However, wider questions remain as to how the relatively simple circuitry of the cerebellum accomplishes its complex and varied functionality (Mitoma et al., 2021).

As it is generally agreed that the core features of the cerebellar module are well conserved across vertebrate phylogeny (Bell et al., 2008; Finger, 1983; Meek, 1998), studies of simpler vertebrates may provide useful perspectives on cerebellar function. The zebrafish has been steadily gaining importance as an experimental model, with behavioral studies dating back to 1960s, the pioneering work on its genetics and development by George Streisinger in the 1980s (Streisinger & Walker, 1983), and especially since 2000 when it has been increasingly used across many disciplines of biology, from genetics to behavioral neuroscience, particularly in investigations of motor function (Fetcho, 2012; Hoxha et al., 2016; Okamoto, 2014). The larval zebrafish has proved especially attractive here because of its much smaller brain size, optical transparency and ease of genetic manipulation. The number of cerebellar Purkinje neurons is about 300 at the larval stage (Hamling et al., 2015; Kalueff et al., 2014; Stewart et al., 2014), compared with 100,000 in adult mice (Herrup & Trenkner, 1987), the model for many cerebellar studies (Ito, 1984; Thompson & Steinmetz, 2009). In larval zebrafish, the activity of the whole cerebellum, or even the entire brain can be monitored during behavioral tests (Ahrens et al., 2012, 2013; Knogler et al., 2017; Lin et al., 2020; Marques et al., 2019; Portugues et al., 2014), while rapidly emerging technologies for mapping circuits and manipulating genetically identified cell types have made targeting of specific cells for modulation and recording especially tractable (Fetcho, 2012; Hoxha et al., 2016; Okamoto, 2014).

Several lines of evidence indicate that the zebrafish cerebellum is functional at larval stages. Developmental studies have shown that by 5 days postfertilization (dpf) the Purkinje cell and granule cell layers of the cerebellar cortex have formed and that the two major input pathways to Purkinje cells—the mossy fiber-granule cell-PF

pathway and the olivocerebellar CF pathway—are in place (Bae et al., 2009; Takeuchi et al., 2015). Electrophysiological studies have demonstrated that larval zebrafish Purkinje cells exhibit both simple spikes and CF responses, with firing patterns that change relatively little after 6 dpf (Hsieh et al., 2014; Sengupta & Thirumalai, 2015; Scalise et al., 2016). Optogenetic activation or silencing of larval Purkinje cells alters swimming movements during the optomotor response (Matsui et al., 2014). It has been also reported that lesioning of the olivocerebellar pathway prevents motor adaptation in a closed-loop, fictive optomotor-response paradigm (Ahrens et al., 2012), and that lesioning of the cerebellum impairs classical conditioning (Aizenberg & Schuman, 2011; Blank et al., 2009; Hinz et al., 2013).

It is unknown, however, to what degree the local circuitry in a larval cerebellum (Bae et al., 2009; Kani et al., 2010) is comparable to its counterpart in the adult fish. This is because cell numbers increase exponentially during the early stages of development (Hibi et al., 2017), and the cerebellum, as well as the whole brain mass, are enlarged significantly (Hamling et al., 2015). Also, at the larval stage, the laminar structure is hardly recognizable (Kaslin et al., 2013; Takeuchi et al., 2015), suggesting that interactions between PF and CF activations, if any, might be different from those found at adult level.

One of the differences found among mammalian Purkinje cells is whether they express high levels of the metabolic enzyme aldolase-C (zebrin II). The immunological visualization of zebrin II in PCs shows their compartmentalization into stripes or bands perpendicular to the lines of PFs across the lobules of the cerebellar cortex (Hawkes & Herrup, 1995). Zebrin II-positive and -negative Purkinje cells have been shown to have distinguishing properties of interaction between their simple and complex spikes (Tang et al., 2017). But Purkinje cells in zebrafish are all zebrin II-positive (Bae et al., 2009), suggesting that they should all be basically the same.

Our investigations reported here and earlier (Han & Welsh, 2014) in an in vitro slice preparation of the adult (>6 month) cerebellum combined with whole-cell patch recording and morphological tracings of labeled single cells show that the zebrafish cerebellum in many ways resembles that of mammals. It remains a laminar structure, consisting of molecular, ganglionic, and granular layers, and its Purkinje cells still receive information from PF and CF inputs. However, its Purkinje cells, rather than being all basically the same, were revealed as remarkably diverse in their physiology and morphology.

A recent ex vivo study fully examined this diversity of Purkinje cells in the corpus cerebelli (central lobe) of adult zebrafish (Chang et al., 2020) and classified them into four subtypes based on their morphology and the responses to current injection of patched cells. It showed further that these Purkinje cells are actively involved in fictive locomotion by demonstrating correlations of Purkinje cell subtype activity with different phases of the swim cycle. The authors also found a similar diversity of Purkinje cell subtypes in the adjacent cerebellar region of the valvula (Chang et al., 2021). We have also found that adult zebrafish Purkinje cells can be classified into at least three subtypes based on both their physiology and morphology, and that these cell subtypes as well as their synaptic inputs can be further characterized pharmacologically. In contrast, eurydendroid cells, the functional equivalent of mammalian DCN cells, which convey all cerebellar signals from Purkinje cells to other parts of the brain, are all similar in their physiology and morphology. Hence, while motor control and motor learning are basic functionality of the zebrafish cerebellum as they are for mammals, the role of the local circuitry of these Purkinje cells subtypes and consequentially its computations are likely to be far less stereotyped and different from those of other known cerebellar models.

2 | MATERIALS AND METHODS

2.1 | General

All recordings were carried out in in vitro slice preparations from the cerebellum of adult zebrafish (*Danio rerio*, >6 month old of either sex). Wide-type (WT) and transgenic Tg*[olig2:RFP]* (obtained from Dr. Cecilia Moens in the UW Biology Department) and Tg[*Ptf1a-GFP]* fish lines were used as noted. The experiments were performed at two sites: the Center for Integrative Brain Research of Seattle Children's Research Institute (SCRI) in Seattle and the Department of Pediatrics and Neuroscience of Xijing Hospital in Xi'an, China. Fish were obtained from local wholesale dealers, pet stores or the Xijing Hospital's Center for Research Animals and were housed and handled according to national and institutional guidelines. All experiments were approved by the Institutional Animal Care and Use Committee of SCRI (IACUC no. 09–0622) or by the Center for Experimental Animals of Xijing Hospital. At SCRI, the zebrafish used in this study were kept in the institutional aquatic facility, where room temperature is maintained at 27–28°C and lights are switched on and off on a 12/12 h cycle. They were cared for by the vivarium staff and handled in accordance with national and institutional guidelines. A total of 80 fish were used for these experiments.

2.2 | Slice preparation

The fish were deeply anesthetized by immersion in tricaine methane sulfonate (MS-222) at a concentration of 100 mg/L. The skin was removed and the skull was opened with fine-tipped forceps. The exposed brain was irrigated with ice-cold low-Na^+ artificial cerebrospinal fluid (ACSF) with composition (in mM) KCl 2.0, KH_2PO_4 1.25, $NaHCO_3$ 24, $CaCl_2$ 2.6, $MgSO_4 \cdot 7H_2$ 0 1.6, glucose 20, sucrose 213. It was then removed and placed in the cold normal ACSF, with the sucrose replaced by equimolar NaCl (see below). In preparing slices, the whole fish brain was glued onto a cutting plate and supported with a gelatin blocker. The cutting chamber was filled with ice-cold low-Na^+ ACSF oxygenated with a mixture of 95% O_2 and 5% CO_2. A low-Na^+ ACSF was used in order to reduce the excitotoxic shock caused by the slicing.

Two 200 μm parasagittal slices were typically obtained from each brain. Each slice contained at least some of the central lobe, where the cerebellum's laminar structure can be easily delineated under a microscope. (In a few cases, transverse slices were also prepared for recordings.) Immediately after cutting, the slices were transferred to a

holding bath, where they were kept submerged at 27 ± 1°C. The ACSF here was a 1:1 mixture of the low-Na^+ ACSF and normal ACSF, where the composition of the latter was (in mM): NaCl 124, KCl 2.0, KH_2PO_4 1.25, $NaHCO_3$ 24, $CaCl_2$ 2.6, $MgSO_4 \cdot 7H_20$ 1.6, glucose 20. The slices were kept in the holding bath for ~30 min and then maintained in normal ACSF at room temperature (21–22°C) until use. Both the low-Na^+ ACSF used in preparing slices and the normal ACSF used during recording were bubbled with 95% O_2 and 5% CO_2 (pH 7.4 ± 0.5, osmolarity 300 ± 5).

2.3 | Recording and stimulation

Individual slices were transferred to a submerged recording chamber. There, they were bathed in a continuous flow of oxygenated normal ACSF preheated at 27 ± 1°C. Single cells were selected randomly for whole-cell patch recording from the ganglionic layer (GaL) of the central lobe. The recording electrodes had resistances of 5–10 MΩ after being filled an internal solution, the composition of which was (in mM): K^+-gluconate 130, EGTA 5, HEPES 10, KCl 3, $MgCl_2$ 2, Na_2 ATP 4, Na_2-phosphocreatine 5, and Na_2-GTP 0.4 (pH 7.4 ± 0.5, osmolarity 280 ± 10). In many cases, the internal solution also contained 0.3–0.5% biocytin (Sigma–Aldrich, St. Louis; B4261) or neurobiotin (Vector Laboratories, CA; SP-1120) to label the recorded cell for later morphological verification.

Cells in the GaL (Figure 1a) were visualized under infrared Nomarski optics using the 40× water-immersion objective of an upright microscope (BX51WI, Olympus; or Axoskop I, Zeiss). Recording electrodes were advanced by a micromanipulator (MP-285 or MP-225; Sutter Instruments, CA), and at the cell membrane, a gigaohm seal was established by a gentle suction. The membrane was then ruptured by additional small negative pressure or zap pulses (0.1–0.5 ms). Recordings were made in both voltage- and current-clamp modes. The recording signals were amplified and digitized and stored in a computer hard drive for offline analysis. A Multiclamp 700A amplifier and Digidata 1322A were used for the recordings, while P-clamp 10 software was used for data acquisition and analysis (all from Molecular Devices, San Jose, CA).

Pairs of stimulating electrodes were used to activate input fibers to induce synaptic responses in patched cells (Figure 1b). To activate PFs, pairs of tungsten electrodes were used, with the stimulating electrode placed in the molecular layer (ML) and the reference electrode in the bath. To activate a Purkinje cell's single CF, theta tubing (tip size <5 μm in diameter) was positioned in the GaL. Typically, the stimulation electrode had to be repositioned multiple times in order to induce an optimal response (particularly an all-or-none response) at the corresponding CF–PC synapse, while the glass tubing significantly reduced the risk of losing the patched PC during repositioning. Negative currents were triggered by TTL signals, typically 0.1 ms in duration and delivered through a stimulus isolation unit. The intensities of the current were adjusted to half of the maximum responses (30–100 μA). Spike amplitudes are reported as resting-potential-to-peak values and spike widths were measured at half the spike's peak amplitude.

Neurobiotin or biocytin tracer was prepared in the internal solution (0.3–0.5%) and kept in the freezer until use. Patch electrodes tips were back-filled with the tracer solution and the remaining portion with normal internal solution. During electrophysiological recordings and pharmacological manipulations, tracer in the patch pipettes was typically diffused into the recorded cells for labeling. If the recording sessions were shorter than 20 min, this process was facilitated by injection of positive current pulses (500 ms on, 500 ms off, 0.5 nA) through the patch pipette for 10–15 min. Slices were fixed overnight in 4% paraformaldehyde in 0.1 M phosphate buffer in final preparation for routine histological procedures (Han et al., 2006).

2.4 | Pharmacology

The following pharmacological agents were used: the glutamate α-amino-3-hydroxyl-5methyl-4-isoxazolepropionic acid (AMPA) receptor antagonist 6-cyano-7-nitroquinoxline-2,3-dione (CNQX; 10 μM); the glutamate N-methyl-D-aspartate (NMDA) receptor antagonist D(-)—2-amino-5-phosphonopentanoic acid (AP5; 30 μM); the $GABA_a$ receptor blocker bicuculline methiodide (30 μM); the Na^+ channel blocker tetrodotoxin (TTX; 1 μM); and the nonspecific Ca^{2+} channel blocker $CdCl_2$ (50–100 μM). All compounds were purchased from Sigm–Aldrich or Tocris unless otherwise noted. The drugs were prepared in stock in DMSO (dimethyl sulfoxide) or distilled water and kept in the freezer until use.

2.5 | Histology

2.5.1 | Single cell labeling

The slices containing cells injected with intracellular tracer were fully rinsed with 0.1 M phosphate buffer plus 0.1–0.5% Triton-X 100, followed by their incubation in 0.5–1.0% streptavidin-conjugated Alexa fluor-594 (Vector Laboratories; A-2006-5) or fluorescein (Vector Laboratories; SA-5488-1) for 2–4 h to visualize the labeled cells in red or green, respectively. In some cases, a Nissl staining with NeuroTrace green fluorescent Nissl stain (Molecular Probes, OR; D21480) was also carried out to visualize the cerebellar laminar structure. After a final rinse in phosphate buffer, the slices were mounted and covered in Vectashield (Vector Laboratories; H1000) for observation under a fluorescent microscope and for imaging under a confocal microscope.

2.5.2 | Drawing and tracing of labeled cells

For cell type identification, labeled cells were imaged on a confocal microscope (Zeiss AxioPlan 2; LSM 510 Meta) at 10× or 20× magnification (0.45 NA or 0.8NA, respectively). Z-stacks of images were acquired at 1.0–1.5 μm z-resolution. For quantitative analysis, the best-labeled cells of each subtype were selected and physiologically identified; then, some of these were imaged on a confocal microscope

with an oil immersion objective (Zeiss Axioplan 2, LSM 510 Meta) at 63× magnification (1.4 NA). Z-stacks of single cell image were acquired at 0.5 µm z-resolution. All image acquisitions were performed with ZEN software (Zeiss, Germany; RRID:SCR_013672). Selected photomicrographs were converted into a 2D image in tiff-format for drawing with a camera lucida. Some were also converted into a 2D 8-bit tiff-format image for digital analysis of cell morphology parameters, including the soma size, length of the primary dendrite and axon, and the total length of the distal dendrites and axon arbors, using the "Simple Neurite Tracer" FIJI software (modified from ImageJ) (Longair et al., 2011; Schindelin et al., 2012).

2.6 | Statistics

Data analysis was carried out using the Clampfit function of P-Clamp 10 (Molecular Devices), along with Origin (OriginLab, Northampton, MA), Prism (GraphPad, San Diego, CA), and CorelDraw (Corel 11, Ottawa, Canada) software. Results are presented as mean ± *SEM*. Statistical comparisons were made with the paired Student's *t*-test, or repeated-measures ANOVA, as noted. *p* Values at .05 and .01 were considered significant and highly significant, respectively.

3 | RESULTS

3.1 | Brief review of zebrafish cerebellar anatomy

The cerebelli of teleosts share a basic functional circuitry (Finger, 1978; Meek, 1998). In adult zebrafish, as shown for a typical parasagittal plane near the midline (Figure 1a), it includes three major parts (from rostral to caudal): the valvula (Val), the central lobe, (CeL), and the caudal lobe (CaL). The Val and CeL have a trilaminar structure, while the CaL appears unstructured, with unidentified cell types located caudally.

It is generally assumed that zebrafish Purkinje cells receive spatially separated PF and CF inputs, while their axons project locally onto neighboring Purkinje cells and eurydendroid cells (Figure 1b). The eurydendroid cells receive inputs from PFs and Purkinje cells, and project outside the cerebellum (Bae et al., 2009; Kani et al., 2010, but see Dohaku et al., 2019). In addition, a set of Purkinje cells project to the VN, which are located in the brainstem (Knogler et al., 2019). The present study focuses on the central lobe, which occupies most of the adult zebrafish cerebellum and is where the vast majority of its principal cells, including Purkinje cells and eurydendroid cells are located.

3.2 | Physiology of adult zebrafish Purkinje cells

The preparations of sagittal slices from the cerebellum of wildtype zebrafish remained healthy typically for multiple hours. The vast majority of our whole-cell recordings were done in the central lobe GaL, which is easily recognized in a sagittal slice due to the region's laminar structure (Figure 1a). The Purkinje cells and eurydendroid cells were generally small (5–8 µm in diameter) and could be visually selected for recording. The small size of these cells required reducing the tip of the patch pipette to have a 6–10 MΩ input resistance after being filled with an internal solution. The physiological features of these cells turned out to be much more complex than expected from the cerebellar literature of mammals (Llinas & Sugimori, 1980a, 1980b) as well as that of the mormyrid (Han & Bell, 2003; Zhang et al., 2011), although the latter is a teleost species, like the zebrafish. We found an unexpected variability in the action potentials, which ranged from ~1 ms to up to 20 ms in duration (all spike widths measured at one-half spike amplitude) and from ~15 to 40 mV in peak amplitude.

In order to better characterize these cells, we combined investigation of their physiology with single-cell morphology by routinely adding the intracellular tracer biocytin or neurobiotin to the patch recording electrodes. A total of over 250 cells were recorded, with more than 60 morphologically labeled, which allowed us to distinguish Purkinje cells from eurydendroid cells (see next section). From this data, we were able to establish criteria for cell identification and classification in the adult zebrafish cerebellum. Accordingly, 161 cells were tentatively classified as Purkinje cells. As shown in Figure 2a, these Purkinje cells fell into three groups based on their spike durations. Mean spike width values for each group were as follows (mean ± *SEM*): Type I, $n = 42$, 1.27 ± 0.63 ms; Type II, $n = 71$, 6.22 ± 1.46 ms; and Type III, $n = 48$, 13.44 ± 5.6 ms. Statistically, the mean spike width for each group was significantly different from that of the other two groups, with one-way ANOVAs between each pair of groups showing clear separations ($p < .01$; Figure 2b). These three groups of Purkinje cells may then be characterized as follows:

3.2.1 | Type I, narrow spike cells

Under current-clamp conditions, these cells had a mean resting membrane potential of −58.7 ± 7.5 mV (mean ± *SEM*, same as below) and fired brief, narrow spikes, with mean spike durations less than 2 ms (Figure 2b). Recordings from one of these narrow-spike cells are shown for current- (top) and voltage-clamp (bottom) conditions (Figure 2c). Spike amplitudes were typically low, with mean spike amplitude 13.5 ± 2.7 mV and no observable overshoot (Figure 3a). The mean input resistance of these cells was 445 ± 134 MΩ (Figure 3b). Many were spontaneously active, while injection of a small current (50–100 pA) through the recording electrode elicited similar narrow spikes in all cells tested.

3.2.2 | Type II, broad spike cells

These cells had a mean resting membrane potential of −61.1 ± 9.5 mV under current clamp and fired spikes with spike durations between 3 and 7 ms, significantly broader than those typically found in neurons in other structures or species. They have hence been classified

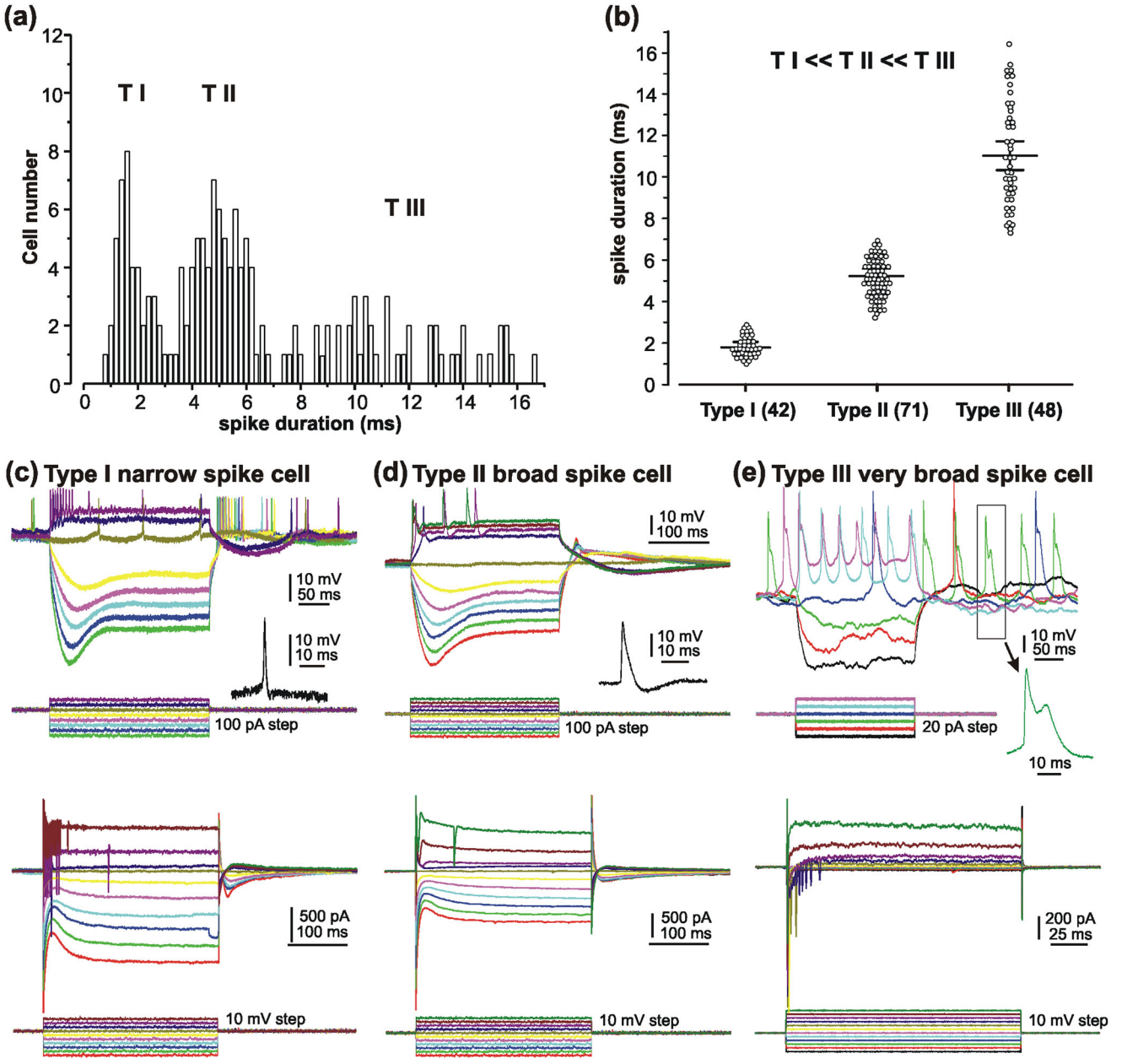

FIGURE 2 Statistical analysis of Purkinje cell physiology. (a) Distribution of Purkinje cell spike durations, with all spike widths measured at one-half spike amplitude. While cells with spike durations <7.0 ms appear to fall into two groups, cells with spike widths >7.0 ms are randomly distributed in a broad range, up to 17.0 ms. (b) Based on the spike durations shown in a, a total of 161 cells have been classified into three groups: Type I, <3.0 ms ($n = 42$); Type II, 3.0–7.0 ms ($n = 71$); and Type III, 7.0–17.0 ms ($n = 48$), with the mean value of each group significantly different from that of the other two ($p < .01$). (c–e) Physiology of representative Purkinje cell subtypes. Top, voltage responses to intracellular current pulses for each Purkinje cell subtype under resting conditions; bottom, current responses to intracellular voltage steps. Current and voltage steps are shown below each panel. Unless otherwise noted, here and in the following figures, voltage responses are recorded from the resting potential and current responses at a holding potential of −60 mV. The inset in each panel on the second row is an example of the corresponding Purkinje cell subtype's typical spike, with widths as follows: (c) Narrow spike cell, spike duration <2 ms in this cell. (d) Broad spike cell, spike duration ~5 ms in this cell. (e) Very broad spike cell, spike duration ~20 ms with two components in this cell.

as *broad spike cells*. Recordings from one of these cells are shown in Figure 2d for current- (top) and voltage-clamp (bottom) conditions. The mean amplitude of these broad spikes was also low, 14.2 ± 4.7 mV without observable overshoot (Figure 3a). Their mean input resistance was 525 ± 166 MΩ (Figure 3b). Some of these cells were spontaneously active. Injection of a moderate current (100–200 pA) through the recording electrode elicited similar broad spikes in all cells tested.

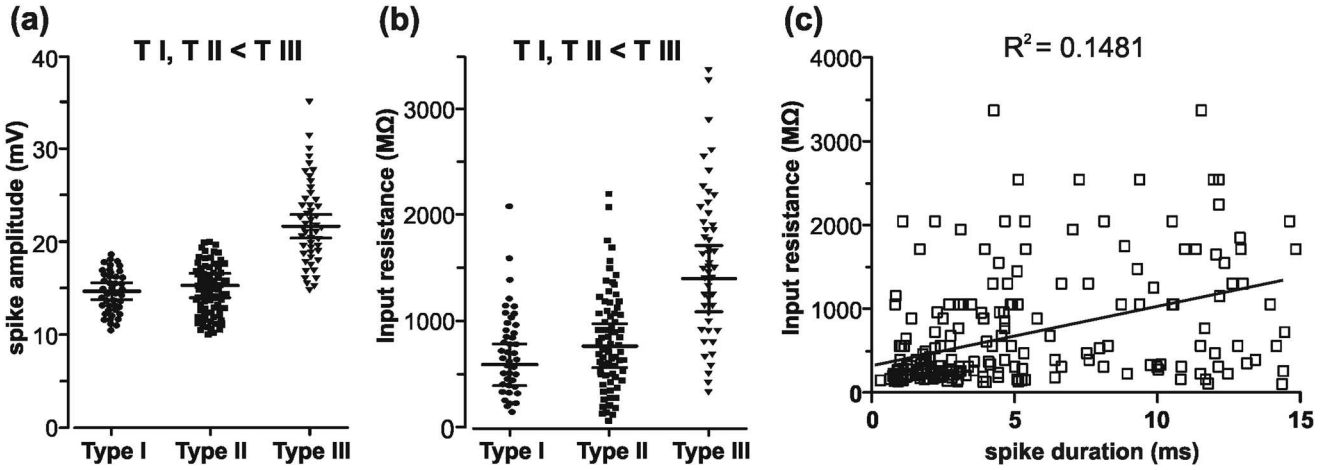

FIGURE 3 Statistical analysis of Purkinje cell physiology. (a) Spike amplitudes in three groups of cells. The mean spike amplitude of Type III cells is significantly higher than that of Types I and II ($p < .05$). (b) Input resistances in the three groups of cells. The mean input resistance of Type III cells is significantly higher than that of Types I and II ($p < .01$). (c) Relation between input resistance and spike duration. The r^2 of 0.1481 indicates that the two parameters are not linearly related ($p > .05$). Note: *Y*-intercept is 321.5 ± 72.24 when $X = 0$

3.2.3 | Type III, very broad spike cells

Under current-clamp condition these cells had a mean resting membrane potential of −63.3 ± 10.9 mV. They fired spikes of variable duration, with spike widths between 6 and 16 ms (Figure 2a), which were significantly broader than those measured for Type I and Type II cells. Hence, these have been named *very broad spike cells* (Figure 2b). Recordings from one of them are shown in Figure 2e for current- (top) and voltage-clamp (bottom) modes. The spikes these cells fired were also variable in amplitude, with a mean spike amplitude of 17.2 ± 9.6 mV and no observable overshoot (Figure 3a). Their mean input resistance was 1135 ± 468 MΩ (Figure 3b). Some very broad spike cells were spontaneously active under resting conditions, while injection of a small current (10–50 pA) through the recording electrode elicited similar spikes in all cells tested.

No difference in resting membrane potential was found between any of these groups of cells (one-way ANOVA, $p > .05$). Spike amplitudes were generally low, with no observable overshoots, as noted above. But while the spike amplitudes were similar for Type I and Type II cells ($p > .05$), those for type III cells were significantly larger (Figure 3a; one-way ANOVA, $p < .05$). As shown in Figure 3b and may also be observed by comparing the voltage-clamp recordings in the bottom panel of Figures 2c and d, the input resistance of the very broad spike cells was significantly higher than that of the narrow and broad spike types. There was no difference in mean input resistance between Type I and II cells ($p > .05$), but values for both types were significantly lower than for Type III cells (one-way ANOVA, $p < .05$) (Figure 3b). The vast majority of the higher input resistance (>1000 MΩ) cells were also found in the Type III group (Figure 2e, bottom). The potential linear relation between input resistance and spike duration is weak or nonexistent (Figure 3c; $r^2 = 0.1481$).

These results indicate that Purkinje cells in the adult zebrafish cerebellum, although very diverse in their electrical properties, can still be classified into three subtypes based on their spike durations. This is in clear contrast to what has been reported for the mammalian (Eccles, 1967; Linas & Sugimori, 1980a, 1980b) and mormyrid (Han & Bell, 2003; Zhang & Han, 2007) cerebellum, in which Purkinje cell physiology is generally much more uniform.

3.3 | Morphology of adult zebrafish Purkinje cells

Our previous work strongly suggests that the combination of cellular physiology and morphology provides useful insight into the functionality of local circuitry in the central nervous system (Han et al., 2006; Shi et al., 2008; Zhang et al., 2018). The diverse physiology of zebrafish cerebellar Purkinje cells characterized above calls for such analysis. Accordingly, the neural tracer biocytin or neurobiotin was routinely added to the internal solution for patch recordings. As the detailed morphology of cells in the adult zebrafish cerebellum has been relatively unexplored, we have adapted morphological criteria for identification of zebrafish Purkinje cells from our previous investigations of the well-characterized mormyrid fish cerebellum, where Purkinje cell somas are located in the GaL, spiny dendritic arbors span the ML, and all axon terminals terminate locally (Han et al., 2006; Shi et al., 2008). Based on these criteria, a total of 59 cells were labeled and identified as Purkinje cells in adult zebrafish cerebellar slices. We then found that, as in the mormyrid cerebellum, the somas and most of the axonal arbors of the labeled cells were located in the GaL. Differing from the mormyrid, however, the dendritic arbors of zebrafish Purkinje cells radiated extremely unevenly into the ML. We used this characteristic patterning of the dendritic arbors to classify zebrafish Purkinje cells into three subtypes.

Type I cells, $n = 11$. These cells have a single primary dendrite that does not branch until reaching the middle of the ML, thereby restricting their dendritic arbors to the outer ML. Typically, the secondary and tertiary branches are initially smooth; then, with their continual branching, they transition into spiny arbors, which occupy the top 40–50% of the ML. One such cell is shown in Figure 4a. Its soma is located in the GaL (Figure $4a_1$), and its axon terminals are largely in the GaL, with a few axon branches extending deeper into the granular layer or oppositely into the ML (Figure $4a_2$). Its distal dendritic arbors are always spiny (Figure $4a_3$). Drawings of two of these type I cells are shown in Figures 5a and b. Physiologically, all eight identified cells were recorded firing narrow spikes, with three others displaying indeterminate electrical activity.

Type II cells, $n = 19$. These cells also have a single primary dendrite in the GaL. However, unlike a type I cell, the primary dendrite of a type II cell branches sparsely at a short distance (~20 μm) from the soma, and then proliferates as a spiny dendritic arbor that spans much of the ML. One of these type II cells is shown in Figure 4b. As with the type I cells, its axon arborization extends beyond the GaL to include terminals in the molecular and granular layers (Figure $4b_2$). Another type II cell is shown in Figure 4c, with its sparse dendritic arbor extending across the whole ML and axon terminals largely in the GaL. Drawings of two of these type II cells are shown in Figures 5c and d. Of these cells 10 were recorded, with seven firing broad spikes, two firing narrow spikes, and the remaining one unclassifiable.

Type III cells, $n = 25$. These cells have one or up to four primary dendrites arising from the soma, which then branch immediately and repeatedly into dense proximal dendritic arbors. These dendritic arborizations, however, were found to have two very different patterns: one largely restricted to the inner half (50–60%) of the ML, and the other spanning the entire ML. We have named these Type IIIa cells ($n = 8$) and Type IIIb cells ($n = 17$), respectively. Representative examples are shown in Figures 4d and e with two drawings of each subtype in Figures 6a and b and 6c and d, respectively. Physiologically, Type IIIa and b cells fired either broad (Type IIIa, $n = 2$; Type IIIb, $n = 3$) or very broad spikes (Type IIIa, $n = 3$; Type IIIb, $n = 6$), with no narrow spikes recorded.

To quantify the Purkinje cell morphology, physiologically identified labeled cells were selected and traced using Image J/Fiji software (Longair et al., 2011; Schindelin et al., 2012). As shown in Figure 7a, the mean values of soma size are similar among the four morphological subtypes (one-way ANOVA, $p > .05$). However, the length of primary dendrites of Type I cells was significantly longer than that of the other types (Figure 7b; one-way ANOVA, $p < .01$), while among the Purkinje cells with shorter primary dendrites, Type II had shorter total dendritic length than Types IIIa and IIIb (one-way ANOVA, $p < .05$). On the other hand, the total length of the dendrites for Type IIIb is significantly longer than that of all other three subtypes (Figure 7c; one-way ANOVA, $p < .05$), but with no difference among the latter three subtypes. The total lengths of the axon arbors in well-labeled cells range from 456 to 1013 μm (668 ± 196 μm, $n = 7$), significantly longer than has been previously reported (Chang et al., 2020; Harmon et al., 2017).

In some cases, multiple cells were recorded and labeled in the same slices. In Figure 8a, a Type IIIa cell and a Type II cell are shown in the same slice, while in Figure 8b, a Type II cell and a Type IIIb cell were labeled in an adjacent area. In another instance, two type IIIb cells were found in the same region (Figure 8c). Finally, two cells, likely Type IIIa, are shown in a transverse slice (Figure 8d), with limited expansion of dendritic arbors in both cells reflecting the orientation of Purkinje cell dendritic trees in the parasagittal plane, as in the mammalian (Ito, 1984; Linas & Sugimori, 1980a, 1980b) and mormyrid cerebellum (Han et al., 2006; Shi et al., 2008).

The approximate soma locations of well-labeled Purkinje cells were plotted in a near-midsagittal plane and a more lateral sagittal plane (Figure 9). It is clear that the Purkinje cell subtypes as morphologically defined are not spatially separated, but instead are found intermingled across the entire central lobe, which is consistent with the labeling of multiple nearby cells of different types shown in Figure 8.

In summary, our results indicate that the morphology of adult zebrafish Purkinje cells, although diverse, may also be categorized into types that roughly correspond to the physiological categories demonstrated previously: Type I cells fire narrow spikes, Type II cells fire broad spikes, and type IIIa and IIIb cells fire either broad spikes or very broad spikes. Our morphological classification is very similar to the one shown in Figure 1k of Chang et al. (2020). Also consistent with their results, we found that these diverse Purkinje cell subtypes were not spatially separated in the central lobe.

3.4 | Responses of Purkinje cells to PF and CF inputs

In the mammalian cerebellum, all excitation of Purkinje cells occurs by way of PF and CF inputs, where the axon terminals of both span the entire ML and each pathway generates a characteristic response that can be duplicated by extracellular stimulation (Konnerth et al., 1990; Perkel et al., 1990). Although recent studies indicate that the Purkinje cells of larvae zebrafish respond to PF and CF inputs (Sengupta & Thirumalai, 2015; Harmon et al., 2017), the corresponding pathways and the responses to their stimulation in Purkinje cells have not been well characterized and have not been investigated at all in the adult zebrafish. We hypothesize that, as in the mormyrid, PF and CF pathways are spatially separated and that the responses of Purkinje cells to PF and CF stimulations are experimentally distinguishable, as has been well-established for the mammalian (Ito, 1984; Linas & Sugimori, 1980a, 1980b) and the mormyrid cerebellum (Han & Bell, 2003; Han et al., 2006; Shi et al., 2008). This hypothesis was tested in slice preparations of the central lobe using physiological and pharmacological approaches.

3.4.1 | PF responses

We examined the responses of Purkinje cells to PF inputs by placing a stimulus electrode in the ML above the patched cell and applying

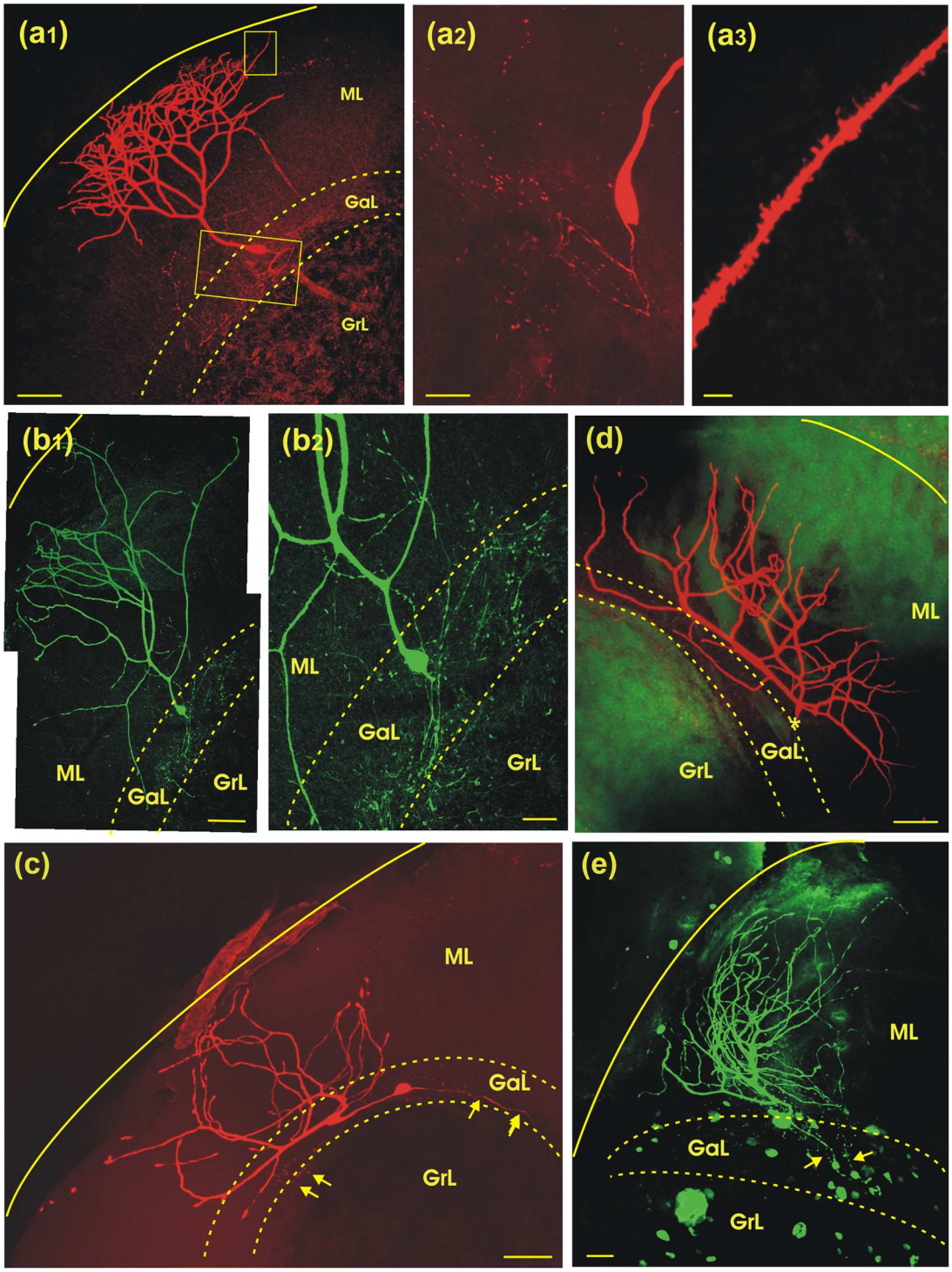

FIGURE 4 Morphology of representative Purkinje cell subtypes, all in sagittal slices. (a) Example of a Type I cell. Its dendritic arborization is restricted to the top half of the ML (a_1), while its axon terminals (shown in an expansion of the large boxed area) are found largely in the GaL, with some in the ML and GrL (a_2). As shown in an expansion of the small boxed area in a_1, Purkinje cell distal dendritic arbors are always spiny (a_3). (b) Example of a Type II cell. Its dendritic arbors radiate across the entire ML (b_1), while its axon terminals are extensive, spreading in the GaL and ML (b_2). (c) Another example of Type II cell, with similar features of dendritic arbors as in b, but with its axon terminals largely restricted to the GaL. (d) Example of a Type IIIa cell. Its dense dendritic arbors are restricted to the lower half of the ML. Note that its soma was lost during retraction of patch pipette and an asterisk indicates its location. (e) Example of a Type IIIb cell. Its dense dendritic arborization extends across the entire ML, with axon terminals largely in the GaL (arrows). Note the abundance of proximal dendrites in the GaL and lower ML for Types IIIa and IIIb, as well as in one of the Type II cell (c), but not in another Type II cell (b) and Type I cell (a). Scale bar = 30 μm in a_1, 10 μm in a_2 and 5 μm in a_3; 30 μm in b_1 and 10 μm in b_2; 50 μm in c; 40 μm in d and 20 μm in e.

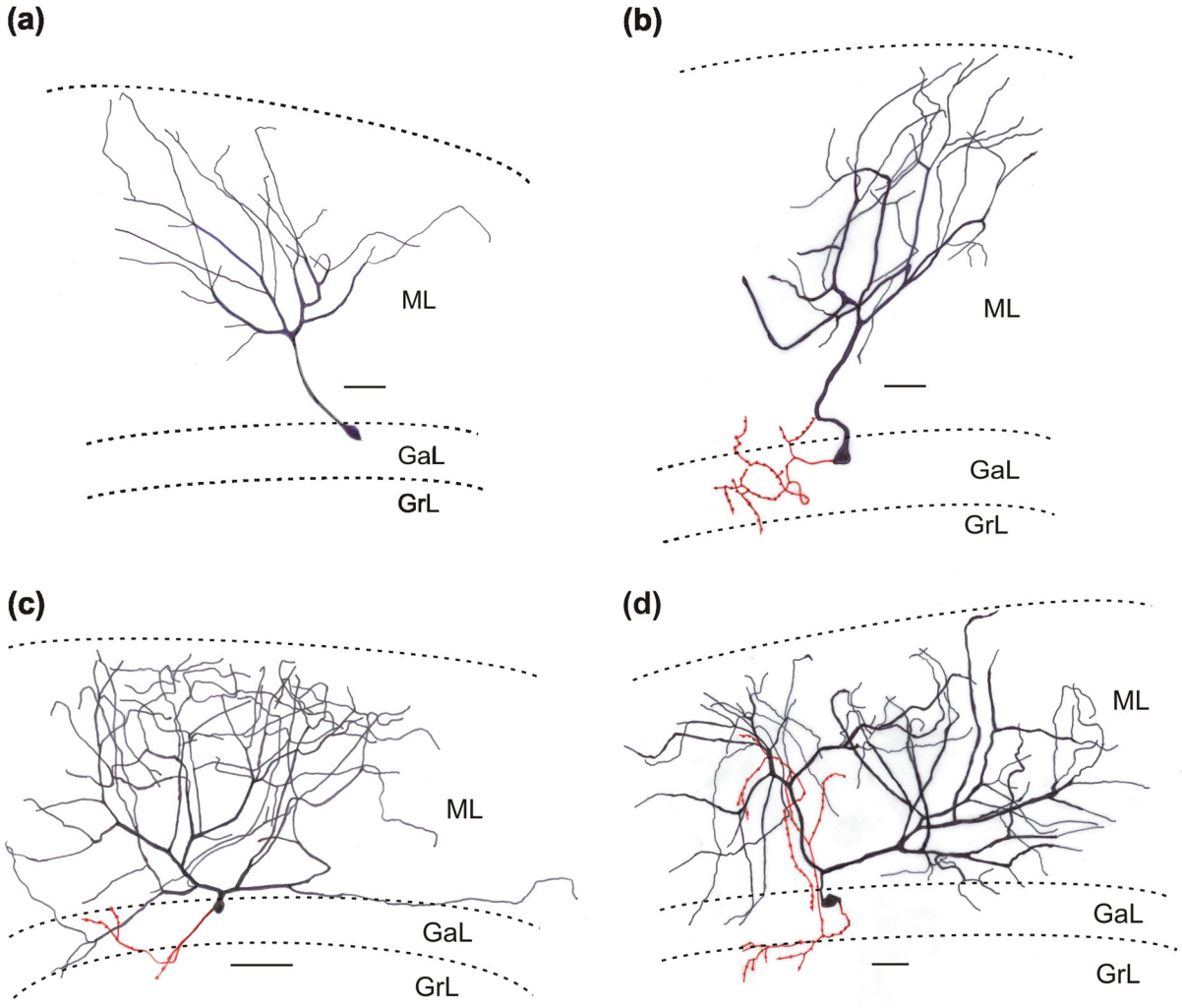

FIGURE 5 Drawings of Types I and II Purkinje cell subtypes in the central lobe from sagittal slices. (a and b) Examples of Type I cells. Note that they lack dendritic branches in the lower third of the ML. (c and d) Examples of Type II cells. Axon arborizations are shown in red. Note that some dendritic arbors are in the GaL and basal ML. Scale bar = 30 μm in a and b; 50 μm in c and 40 μm in d.

brief current pulses (Figure 1b). Repositioning of the stimulus electrode was often required to elicit and optimize the responses. As shown in Figures 10a and b, these responses were graded and showed paired-pulse facilitation (PPF) under both voltage- and current-clamp conditions, as has been also shown to occur in the mammalian (Konnerth et al., 1990; Perkel et al., 1990) and mormyrid (Han & Bell, 2003) cerebellum. Similar results were obtained in 6 cells tested. Pharmacological tests were then performed in either current- or voltage-clamp mode for further characterization of the synapse. Here, it was found that the responses were not affected by bath application of the NMDA receptor antagonist AP5 (30 μM) (3.3 ± 0.44 vs. 3.4 ± 0.66 mV, $n = 5$, $p > .05$), but disappeared in the presence of the AMPA receptor antagonist CNQX (20 μM) (3.4 ± 0.44 vs. 0.3 ± 0.16 mV, $n = 5$, $p < .05$), as is shown in Figure 10c. In another two cells, CNQX (20 μM) abolished the response to PF stimulation without additional AP5 (not shown).

These results indicate that in the zebrafish cerebellum, PFs release glutamate, which excites Purkinje cells via AMPA-, but not NMDA-type receptors, as has been reported for the mammalian (Konnerth et al., 1990; Perkel et al., 1990) and mormyrid (Han & Bell, 2003; Zhang & Han, 2007) cerebellum.

3.4.2 | CF responses

Responses of Purkinje cells to CF inputs were expected in the adult zebrafish cerebellum, as they have been shown to occur in zebrafish larvae (Sengupta & Thirumalai, 2015; Harmon et al., 2017). Indeed, high-amplitude spikes similar to those seen at the larval stage (Harmon et al., 2017) were also seen in some adult Purkinje cells under resting conditions (Figure 11a).

While detailed information is lacking for adult zebrafish Purkinje cells as to the distribution of CF terminals, we repositioned the stimulus electrodes from the ML used to stimulate PFs to the adjacent ganglionic or granular layer. It then became clear that CF responses similar to those in Figure 11a could only be elicited

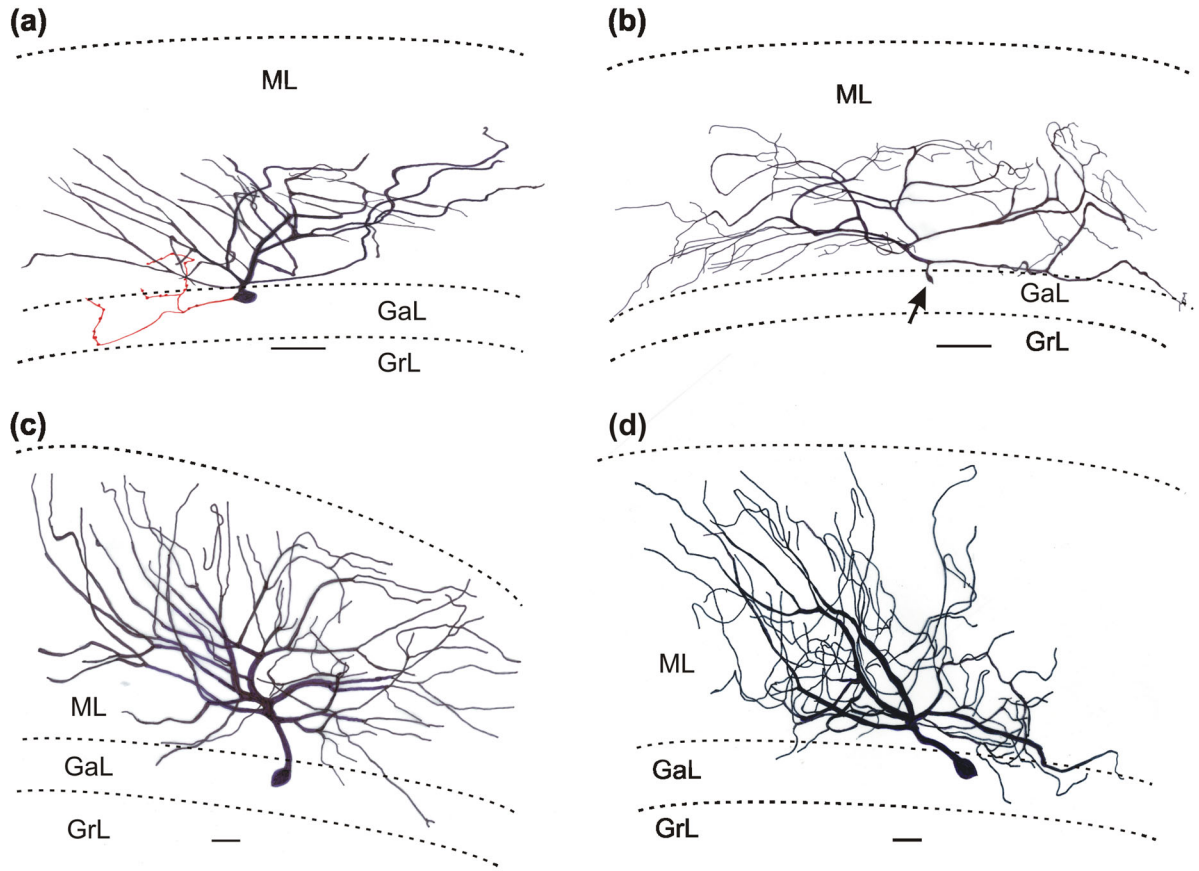

FIGURE 6 Drawings of Types IIIa and IIIb Purkinje cell subtypes in the central lobe from sagittal slices. (a) Example of a Type IIIa cell, with its axon arborization shown in red. (b) Another Type IIIa cell. Its axon was truncated, as indicated by an arrow. (c and d) Example of Type IIIb cells. Note that some dendritic arbors are in the basal ML for Type IIIa cells (a and b), while Type IIIb cells have extensive dendritic arbors in both the GaL and basal ML (c and d). Scale bar = 50 μm in a and b; 30 μm in c and d.

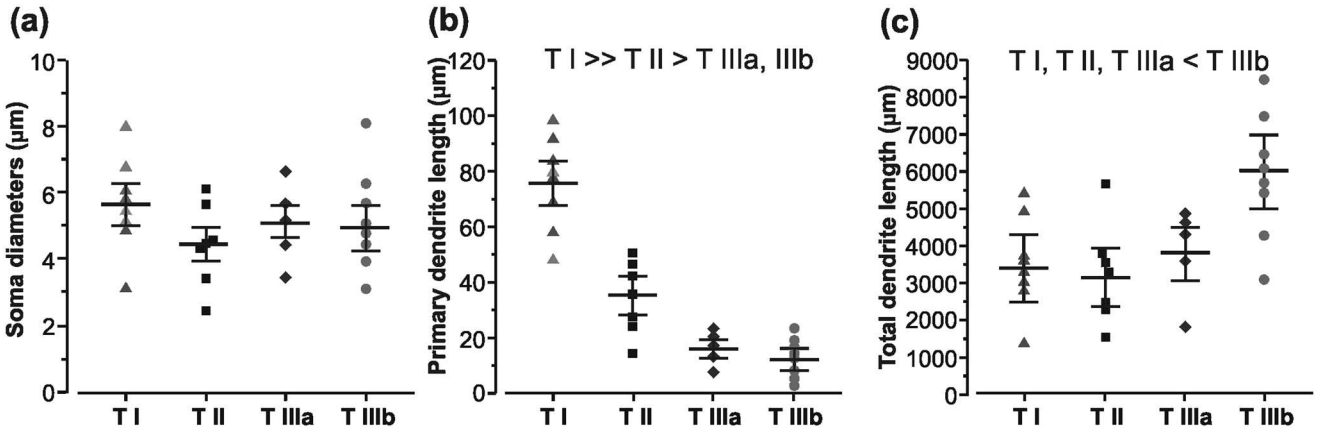

FIGURE 7 Statistical analysis of Purkinje cell subtype morphology. Confocal images of labeled cells were selected and traced with an aide of Fiji/Image J. (a) Soma size. While the soma diameters are variable, there is no significant difference between cell types ($p > .05$ between each pair). (b) Length of primary dendrites. There is no difference between Type IIIa and IIIb ($p > .05$), but Type I and Type II are significantly different from other subtypes ($p > .05$ between each pair). (c) Total length of dendritic arbors. Type IIIb dendritic trees are significantly longer than those of the other cell types ($p < .05$), for which there is no significant difference ($p > .05$).

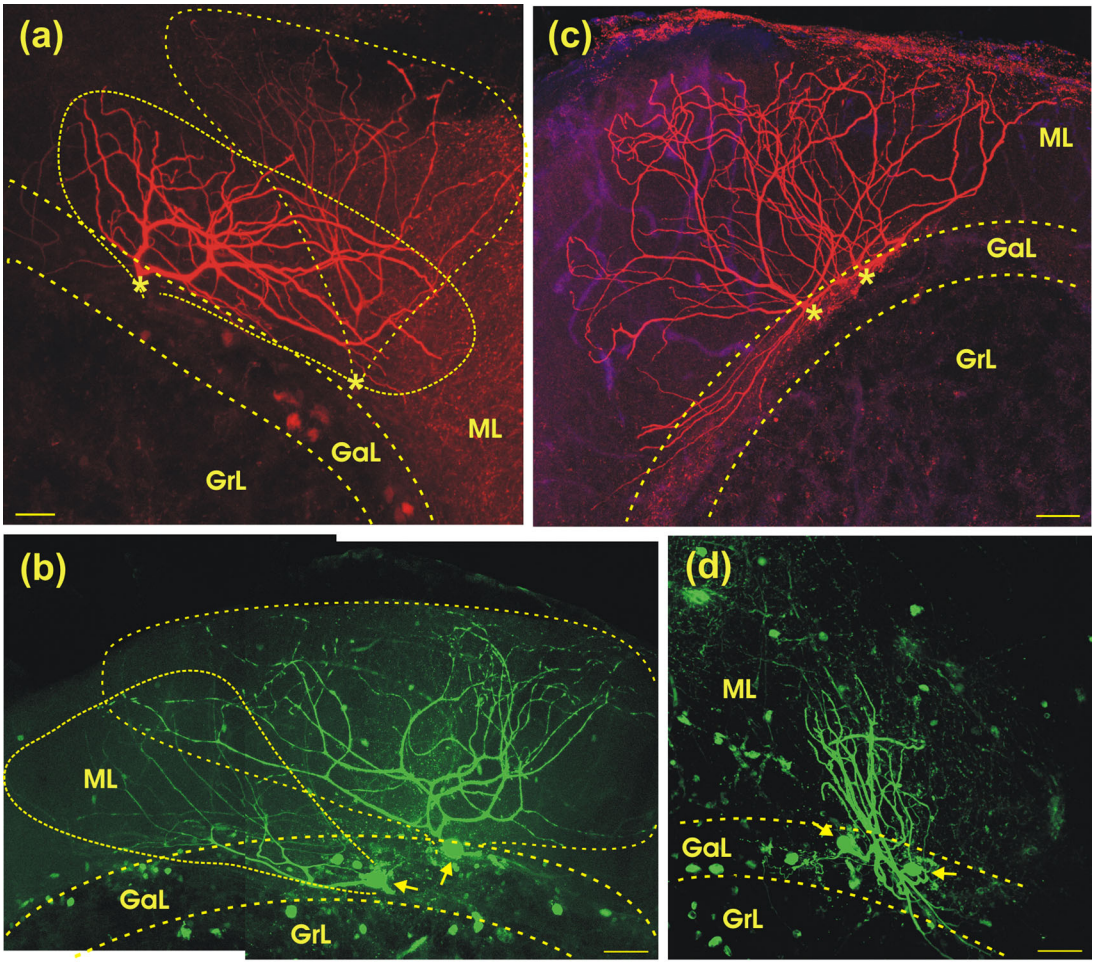

FIGURE 8 Morphology of representative Purkinje cell subtypes found near each other in central lobe sagittal slices (except for d, which is from a transverse slice). Multiple cells in the same region were recorded and labeled in the same slices. (a) A Type IIIa cell (left) and a type II cell (right). (b) A Type II cell (left) and a Type IIIb cell (right). (c) Two Type IIIb cells, with somas nearby each other. (d) Two Type IIIa cells in a transverse slice. Soma locations are indicated by asterisks in a and c. Dashed lines show the approximate boundary of each cell's dendritic tree in a and b. Scale bar = 20 μm in a and b, 30 μm in c and 25 μm in d.

when the stimulus electrode was positioned very close to the patched cell soma in the GaL, but not in the laminae on either side. To optimize responses, repositioning of the stimulus electrode was typically required and stimulus intensities were carefully adjusted to activate the single CF.

Interestingly, Purkinje cell responses to this targeted CF stimulation took two forms of spiking in whole-cell patch recording. Under current clamp, the first type of spike had a waveform consisting of a brief large phase and a long-lasting smaller one. Spiking of this type was all-or-none and showed pair-pulse depression (Figure 11b, top), as has been reported for the CF response in the mammalian (Konnerth et al., 1990; Perkel et al., 1990) and the mormyrid (Han & Bell, 2003; Shi et al., 2008) cerebellum. In voltage-clamp mode, the response to CF stimulation was similar to its counterpart in mammals (Konnerth et al., 1990; Perkel et al., 1990), and was abolished by bath application of CNQX (20 μM). Similar results were obtained from six cells (630 ± 50 vs. 25 ± 15 pA, $p < .05$), an example of which is shown in Figure 11b (bottom). In addition, all but one of these cells fired the broad spikes characterized earlier (Figure 2d). In the subsequent morphological analysis, three of these six cells were successfully recovered and, as their labeling revealed them to have dendritic arbors across the ML, classified as Type II cells (Figures 5c and d).

The second type of spike generated by CF stimulation consisted of complex-like spikelets under current-clamp conditions (Figure 11c, top). Like the Type II cells above, these responses were also all-or-none and paired-pulse depressed. They were also unaffected by the presence of AP5 (30 μM) (840 ± 120 vs. 890 ± 86 pA, $n = 5$, $p > .05$), but disappeared when CNQX (20 μM) was subsequently applied to the bath (Figure 11c, bottom). Similar pharmacological results were obtained in the five cells tested (910 ± 104 vs. 35 ± 46 pA, $n = 5$, $p < .05$). In another three cells, direct application of CNQX (20 μM) completely abolished the all-or-none responses without additional AP5 (not shown). Out of seven cells tested, six fired very broad spikes while another fired broad spikes. In addition, among the six cells recovered for morphological analysis, all had dense proximal dendritic arbors. However, the dendritic arbors of two were restricted to the inner ML (Type IIIa; Figures 6a and b), while those of the other four spanned the entire ML (Type IIIb; Figures 6c and d). None of these cells

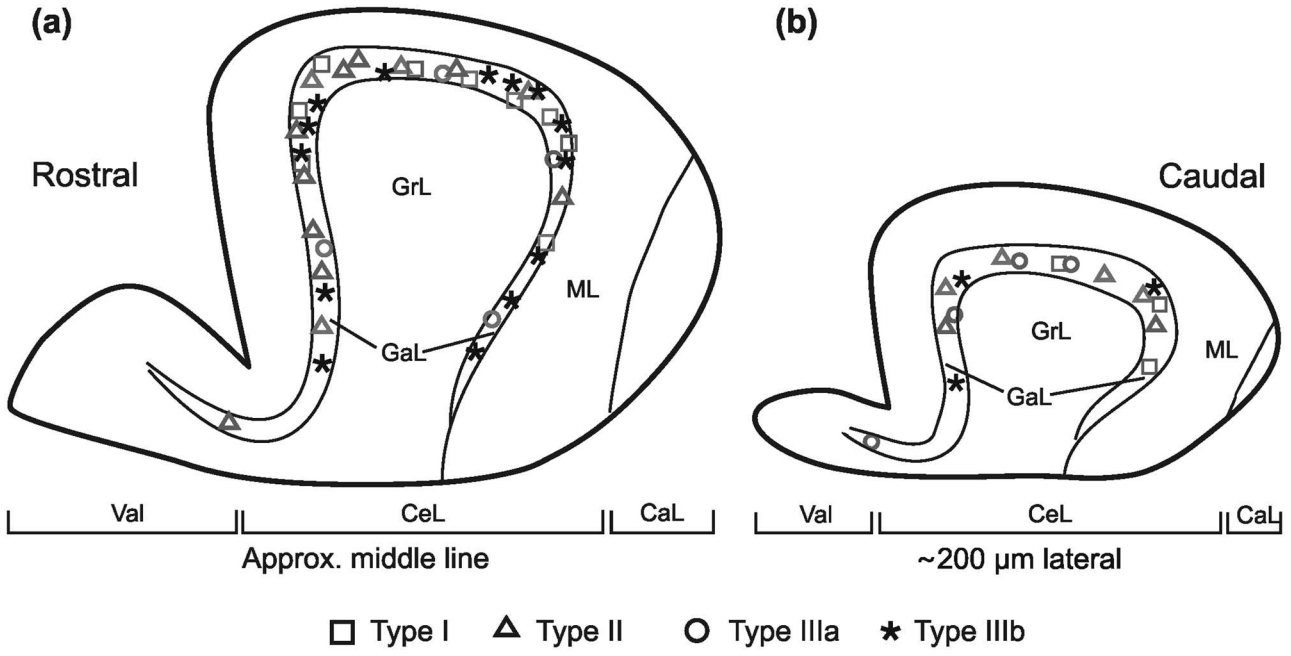

FIGURE 9 Schematic illustration of Purkinje cell soma distribution in the parasagittal planes of the central lobe. Two representative planes are shown, one at the approximate midline (top) and another about 250 µm lateral (bottom). Only cells that were physiologically and morphologically identified (see text) are shown, with the majority located in the central lobe and a few in the valvular ridges (Val). These Purkinje cell subtypes exhibited no consistent distribution pattern. CaL, caudal lobe; CeL, central lobe; GaL, ganglionic layer; GrL, granular layer; ML, molecular layer; Val, valvular ridge.

having the all-or-none responses characteristic of CF activation could be morphologically identified as type I cells (Figures 5a and b).

In summary, the responses of zebrafish Purkinje cells to CF activation can be easily identified in whole-cell patch recording. These responses are typically larger than somatic action potentials, are all-or-none and paired-pulse depressed, and are mediated via glutamate AMPA-type receptors, as in mammals (Konnerth et al., 1990; Perkel et al., 1990) and the mormyrid (Shi et al., 2008; Zhang & Han, 2007). Despite repeated attempts, an all-or-none response to CF stimulation could not be induced in some of Purkinje cells tested. This, in addition to variations in the waveforms of CF responses and in the dendritic morphology of Purkinje cells described above, suggests that CF responses of zebrafish Purkinje cells are not uniform, as has been recently hypothesized for Purkinje cells in mammals (Zang & De Schutter, 2019).

3.5 | Pharmacology of Purkinje cell spikes

We next examined the ionic basis of the Purkinje cell spikes using pharmacological tools. First, it was found that narrow spikes could occur spontaneously or be evoked by small inward current steps (20–50 pA; Figure $12a_1$) and were not affected by bath application of the nonselective Ca^{2+} channel blocker $CdCl_2$ (100 µM; Figure $12a_2$). The narrow spikes, however, did disappear after a subsequent addition of the Na^+ channel blocker TTX (1 µM; Figure $12a_3$). Similar tests were performed in four cells with consistent results. In another two cells, TTX (1 µM) was bath applied without the $CdCl_2$, and the spikes were also blocked (not shown). These results indicate that the narrow spikes fired by Type I Purkinje cells are Na^+ spikes, similar to those found in all central neurons.

We then tested broad spike cells using similar procedures. As shown in Figure 12b, broad spikes, like narrow spikes, occurred either spontaneously or in response to the injection of inward current steps (Figure $12b_1$, inset). After bath application of TTX (1 µM), broad spikes could still be evoked by injection of a higher intensity of inward current (~200 pA), but their waveform was clearly changed, with the rising phase becoming significantly longer, from ~1 ms to above ~10 ms (Figure $12b_2$). With the further addition of $CdCl_2$ to the bath (100 µM), the altered broad spikes were completely blocked (Figure $12b_3$). Similar tests were carried out in 6 cells with consistent results, indicating that the broad spikes characteristic of zebrafish Purkinje cells include both Na^+ and Ca^{2+} components.

Finally, similar tests were carried out in very broad spike cells. Examples of their responses to drug application are shown in Figure 12c, for which dual-cell recordings were performed on two adjacent cells. Under resting conditions, both cells spontaneously fired very broad spikes, although with slightly different waveforms (Figure $12c_1$). Bath application of $CdCl_2$ (100 µM) completely blocked the spikes of cell B, while revealing components of the ones fired by cell A that resemble narrow spikes (Figure $12c_2$). The latter were then abolished by addition of TTX (1 µM) (Figure $12c_3$). These results indicate that very broad spikes are a type of Ca^{2+} spike that may, in some cases, also include a Na^+ component.

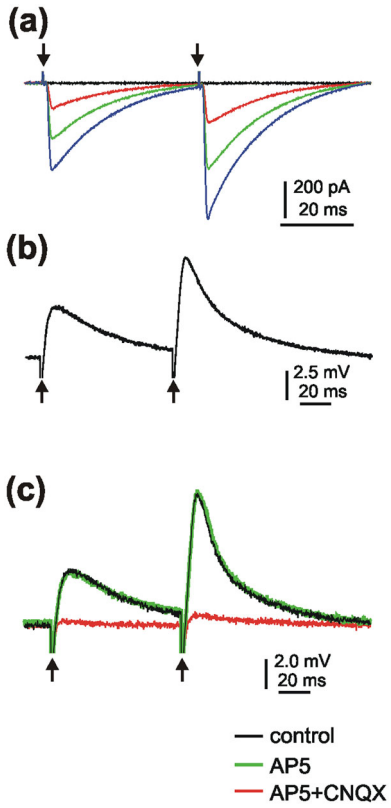

FIGURE 10 Responses of Purkinje cells to PF stimulation. Stimulation electrodes were positioned in the ML to activate PFs. Arrows indicate stimulus artifacts. (a) Paired-pulse responses of a Purkinje cell in voltage-clamp mode, showing graded responses and paired-pulse facilitation. (b) In current-clamp mode, similar stimuli elicit paired-pulse facilitation. (c) Pharmacology of PF responses. PF responses were unaffected by NMDA receptor antagonist AP5 (30 μM), but abolished by further addition of AMPA receptor blocker CNQX (20 μM).

In summary, zebrafish Purkinje cells spontaneously fire at least two types of spikes, a narrow Na^+ spike and a broad Na^+ and Ca^{2+} spike, where variations in the form of the latter are likely correlated with differences in Purkinje cell morphology.

3.6 | Eurydendroid cell physiology

In the mammalian cerebellum, GABAergic Purkinje cells project to DCN cells and the VN, which in turn convey cerebellar information to premotor structures and other brain regions. In teleosts, including zebrafish, Purkinje cells are intermingled with their target eurydendroid cells (Finger, 1978; Han et al., 2006; Ikenaga et al., 2005; Meek, 1998). Reflecting the presence of these projection cells, the Purkinje cell layer has been renamed the *GaL* in teleosts (Meek, 1998). Eurydendroid cells have been examined in detail in mormyrid cerebellum (Han & Bell, 2003; Shi et al., 2008; Zhang & Han, 2007), but little is known about them in zebrafish, particularly at the adult stage. Therefore, we examined the physiological and morphological features of eurydendroid cells in slice preparations of wildtype and *olig2* zebrafish

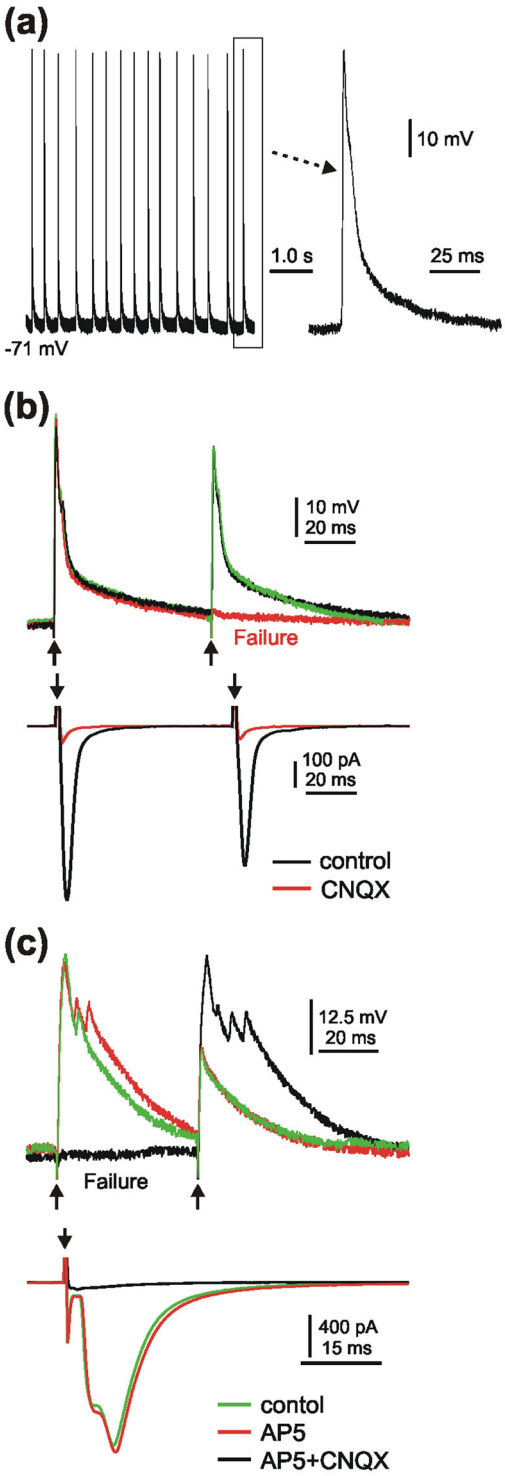

FIGURE 11 Responses of Purkinje cells to CF stimulation. Stimulation electrodes were positioned near the recorded cell in the GaL and then repositioned to find a large, all-or-none response to stimuli at minimal intensity. Solid arrows indicate stimulus artifacts. (a) Spontaneous activity of a broad spike cell, presumably all-or-none in response to CF input at the resting membrane potential −71 mV. (b) Voltage (top) and current (bottom) responses evoked in a broad spike cell in current- and voltage-clamp modes, respectively. The stimulus electrode was placed only in in the GaL. The all-or-none responses are similar to those shown in A. They also demonstrate a

(Continues)

FIGURE 11 (Continued)
paired-pulse depression and are sensitive to the AMPA receptor blocker CNQX (20 μM). (c) Very broad spike cell responses, generated by stimulation similar to that in B, but consisting of multiple components or complex-like spikelets. These responses are also all-or-none, paired-pulse depressed (top), and are insensitive to NMDA receptor antagonist AP5 (30 μM), but abolished by AMPA receptor blocker CNQX (20 μM) (bottom).

lines, using experimental procedures similar to those described above for Purkinje cells.

In the wildtype fish, a total of 13 cells were classified as eurydendroid cells based on their physiological properties; three of these were well labeled and all were all identified morphologically (see below). Typically, their spikes were narrow (≤2 ms) and had high amplitude peaks that sometimes overshot (≥50 mV), followed by a brief after-hyperpolarization potential (AHP). Rebound discharges—bursts of spikes following an inward current step—were often present, although variable in duration. These zebrafish eurydendroid cell spikes are similar to those of their counterparts in mammalian DCN (Han et al., 2014; Sarnaik & Raman, 2018) and in the mormyrid (Han & Bell, 2003; Shi et al., 2008) cerebellum. Recordings from one such cell are shown in Figure 13a.

Our earlier experiments indicated that the probability of recording from wildtype zebrafish eurydendroid cells was less than 10%. Fortunately, both larval and adult zebrafish express the transcription factor *olig2*, which gives rise to oligodendrocytes and specific types of neurons (McFarland et al., 2008; Bae et al., 2009). The latter include eurydendroid cells, which can then be physiologically identified (Heap et al., 2013; Harmon et al, 2020). In zebrafish from the *Tg[olig2:RFP]* line, a set of eurydendroid cells were genetically labeled with fluorescent indicator and could then be easily selected for recording. Figure 13b shows recordings from one of 35 such cells we identified in the GaL. It is clear that its physiological properties are different from those of any of the Purkinje cell subtypes described above (Figure 2), and are instead very similar to those of the wildtype eurydendroid cell shown in Figure 13a.

Responses of eurydendroid cells from the wildtype (Figure 13a) and olig2 (Figure 13b) zebrafish lines to the activation of PFs were very similar and are described together here. Using PF stimulation procedures similar to those used for Purkinje cells, EPSPs or EPSCs could be easily induced, which were graded and showed PPF (Figure 13c, top). The responses to PF stimulation were clearly reduced by bath application of the NMDA receptor blocker AP5 (30 μM) (10.3 ± 0.24 vs. 7.2 ± 0.78 mV, $n = 6$, $p < .05$) and completely abolished by further addition of the AMPA receptor blocker CNQX (20 μM) (7.3 ± 0.41 vs. 0.48 ± 0.16 mV, $n = 4$, $p < .05$). These results (Figure 13c) are similar to those seen in the DCN cells of mammals (Han et al., 2014) and the eurydendroid cells of the mormyrid (Shi et al., 2008). In addition, the spikes of these cells disappeared following bath application of TTX (1 μM, $n = 5$), as shown in Figure 13d. In three additional cells, the narrow spikes remain unchanged when the nonselective Ca^{2+} channel blocker Cd^{2+} was applied, but abolished in the additional presence of TTX (1 μM) (not shown). Furthermore, when stimulus electrodes were carefully positioned in the GaL near the patched cells, no all-or-none responses were obtained in all 10 cells tested, consistent with their absence of CF input. These data indicate that similar to mormyrid, at least one set of cells in the GaL of the zebrafish cerebellum is physiologically and pharmacologically distinguishable from Purkinje cells.

3.7 | Eurydendroid cell morphology

Following procedures similar to those previously discussed for Purkinje cells, three cells in a wildtype zebrafish preparation were successfully labeled after their physiological characterization as eurydendroid cells. One of these is shown in Figure 14a. Its dendritic tree was largely oriented in the parasagittal plane and its dendrites were entirely spineless (not shown), while its axon was traced up to 60 μm through the GaL to the granular layer without branching or local terminals. These morphological features are similar to those of the eurydendroid cells we have previously characterized in the mormyrid fish cerebellum (Han et al., 2006).

While fluorescent cells could be easily selected for recording in the *Tg[olig2:RFP]* fish slices, their labeling was, in general, incomplete. Therefore, biocytin or neurobiotin was used as with the wildtype fish to label these cells for morphological characterization. Of the cells we recorded, 15 were found well-labeled; examples are shown in Figures 14b–e. To further verify them as eurydendroid cells, we followed the approach used previously for the morphological identification of Purkinje cells. As with the eurydendroid cells from wildtype zebrafish, those from the *olig2* line typically have somas located in the GaL. Their dendritic trees crossed the entire ML and are largely oriented in the parasagittal plane. All dendritic arbors, if visible, were smooth, as shown in Figure 14e$_{2 \text{ and } 3}$. Their axons were usually thick (likely myelinated) and could be traced up to 170 μm along the GaL or into the granular layer (Figures 14b, c, and e). It is interesting that in several cases the dendritic arbors were found to radiate crossing the ML and then reach the top surface of the tissue before returning to the ML. An example of such morphology is shown in Figure 14b. In addition, six of labeled *olig2* cells were traced similarly as described above for Purkinje cells. Interestingly, their mean soma size (11.1 ± 1.6 μm in diameter) is statistically larger than that of Purkinje cells (7.4 ± 3.6 μm in diameter, $n = 22$; t-test, $p < .05$) and the total length of their dendritic trees ranges from 3.043 to 12.161 mm (5.439 ± 3.454 mm, mean ± *SD*).

Taken together, these results indicate that the eurydendroid cells of the zebrafish cerebellum are physiologically and morphologically distinguishable from adjacent Purkinje cells by their uniformly overshooting spikes and by their rebound discharges in response to hyperpolarization, as well as by their having smooth dendritic arbors and axons that do not project locally. In addition, these cells receive PF input, while CF input is unlikely. These properties are similar to those found in other teleosts, including the mormyrid (Finger, 1978; Han & Bell, 2003; Ikenaga et al., 2005; Meek, 1998), and to those of mammalian DCN cells (Han et al., 2014).

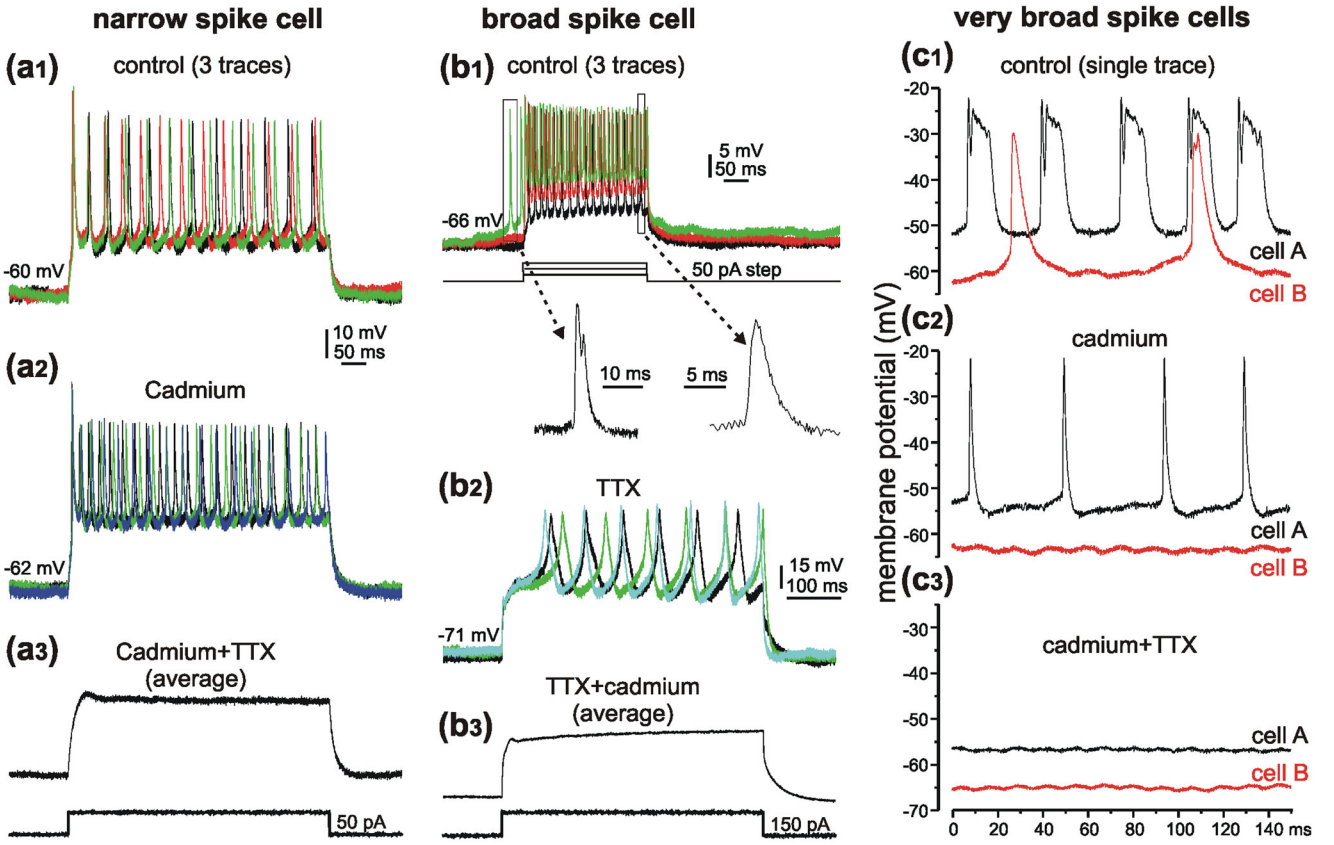

FIGURE 12 Pharmacology of Purkinje cell spikes. (a) Example of a narrow spike cell. (a_1) Inward current injection evokes narrow spikes only, even at higher current steps, 200 pA (not shown). (a_2) The spikes are not affected by the Ca^{2+} channel blocker $CdCl_2$ (100 μM). (a_3) The spikes are abolished following bath application of the Na^+ channel blocker TTX (1.0 μM). (b) Example of a broad spike cell. (b_1) The cell fires broad spikes spontaneously or evoked by current injections in a voltage-dependent fashion. Note the variation in spike waveform between the spontaneous and evoked responses (inset). (b_2) The broad spike waveform is altered in the presence of TTX (1.0 μM). (b_3) The remaining broad spikes disappear following addition of $CdCl_2$ (100 μM) to the bath. (c) Example of a dual cell recording from very broad spike cells. (c_1) Both cells fire very broad spikes spontaneously at resting conditions. (c_2) Very broad spikes disappear in both cells after bath application of $CdCl_2$ (100 μM), but the narrow spikes in cell A remain. (c_3) The remaining narrow spikes in cell A disappear following addition of TTX (1.0 μM) to the bath.

4 | DISCUSSION

4.1 | Major findings

In the adult zebrafish, cerebellar Purkinje cells are remarkably diverse in their physiology and morphology and can be classified into at least three subtypes accordingly. The Type I or *narrow spike cell* fires narrow (<3 ms) Na^+ spikes. Its single primary dendrite arises from the soma and branches only in the distal half of the ML. The Type II or *broad spike cell* fires broad (~5 ms) spikes, each of which include a Na^+ and a Ca^{2+} component. The primary dendrite of the broad spike cell arises from the soma and branches at a short distance, with the secondary dendrites and their arbors extending throughout the ML. The Type III or *very broad spike cell* fires very broad (≥10 ms) spikes, which, like the Type II cell, includes Na^+ and Ca^{2+} components. Single or multiple primary dendrites arise from soma and then branch immediately and repeatedly. This group of cells can be further classified into two subtypes based on their dendritic morphology. The dense dendritic arbors of Type IIIa cells are restricted to the inner half of the ML, while those of Type IIIb cells extend across the entire ML. These two subtypes of Type III cells, however, are indistinguishable physiologically. The rich diversity of adult zebrafish Purkinje cells discovered here is unexpected and in clear contrast to what has been described for the cerebellum of mammals or other examined vertebrates, where all Purkinje cells have been found similar in their physiology and morphology.

Our morphological classification is consistent with the recent report by Chang et al. (2020), in which four subtypes of Purkinje cells were also identified (Chang et al.'s Figure 1k). Neither study found any topographical segregation of these subtypes (our Figure 9; Chang et al.'s Figure 1l and 1o). While similar experimental procedures were used for cell labeling in both investigations, our results provide significantly more morphological detail of Purkinje cells, particularly of their dendritic arbors and axon terminals. The extreme morphological variation of zebrafish Purkinje cell dendrites is likely to be a main determinant of how these cells receive PF inputs selectively (Figure 15).

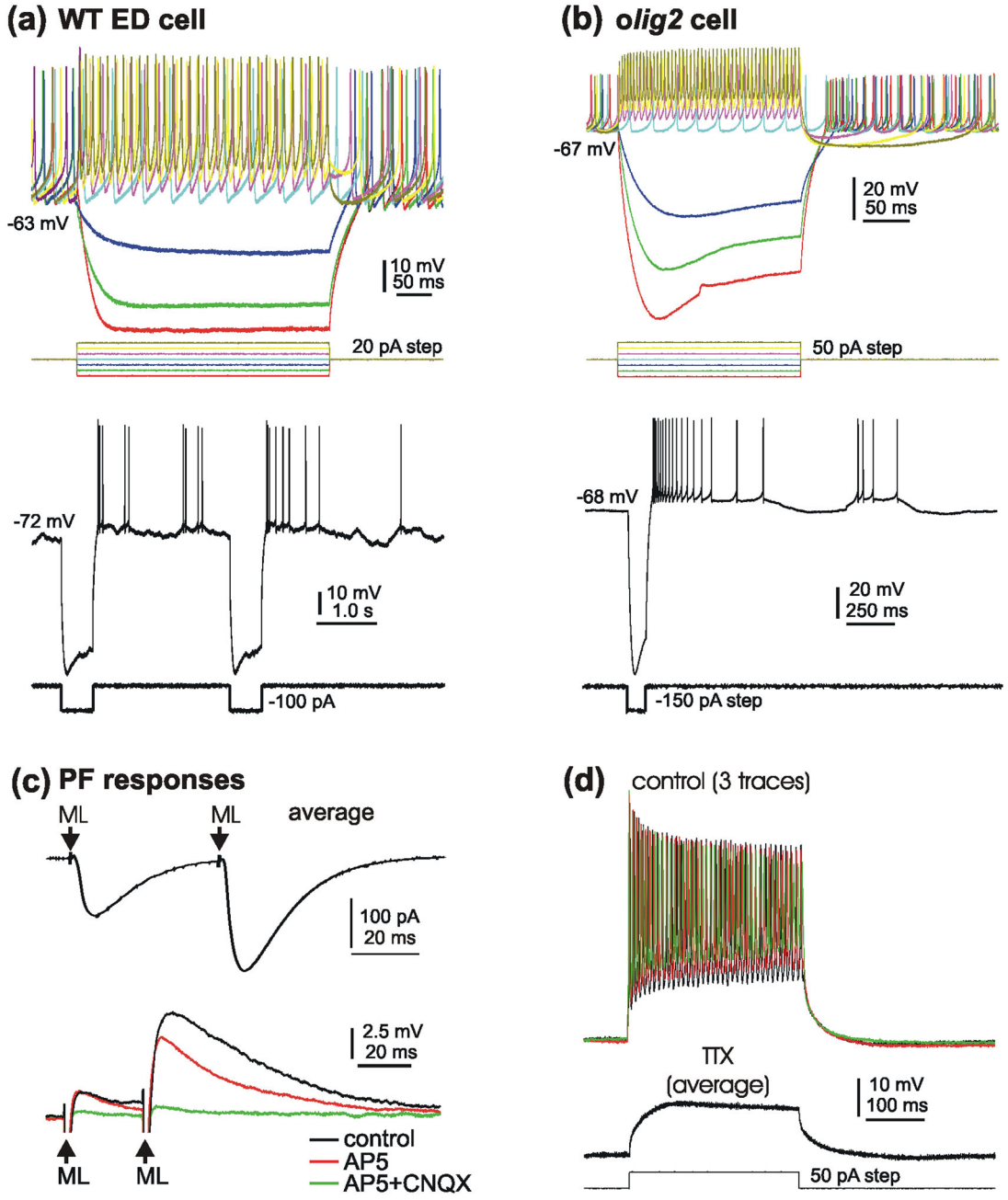

FIGURE 13 Physiology of eurydendroid cells. (a) Example of a eurydendroid cell, which was "blind" patched and classified based on its physiology and morphology. Its spikes, spontaneous or evoked, differ from those of the Purkinje cell subtypes shown in Figure 12 in terms of their uniform shape (top) and rebound discharges (bottom), both were reported in the deep cerebellar nuclear (DCN) cells of mammals. (b) Example of a fluorescently labeled *olig2* cell, showing responses to injected current steps similar to those of the eurydendroid cell in A. (c) Example of an efferent cell responding to PF stimulation. Under either voltage- (top) or current-clamp (bottom) conditions, PF activation induces paired-pulse facilitation, which was reduced by AP5 (30 μM) and abolished by additional CNQX (20 μM), as reported for mammalian DCN cells. (d) Example of efferent cell spikes, which are abolished by bath application of TTX (1.0 μM).

Physiologically, the four subtypes of cells were identified by Chang et al. (2020) based on the adaptation of their spikes to sustained depolarizing current. The decreasing number of induced spikes seen across the first three panels of Chang et al.'s Figure 1c is particularly striking when compared with our analogous Figures 2c–e in which we have characterized three types of Purkinje cells in terms of the response of their electrical activity to current steps. In both classification schemes, spike adaptation is highest for Type I and decreases for Type II, with Type III being basically nonadapting. Unlike the approach of Chang et al. (2020), which uses principle component analysis of a large number of morphological and physiological parameters to establish a quantitative categorization corresponding to these broad differences in spike adaptation (Chang et al.'s Figure 1l), our physiological classification is based mainly on spike width (our Figures 2a and b): the duration of the spikes

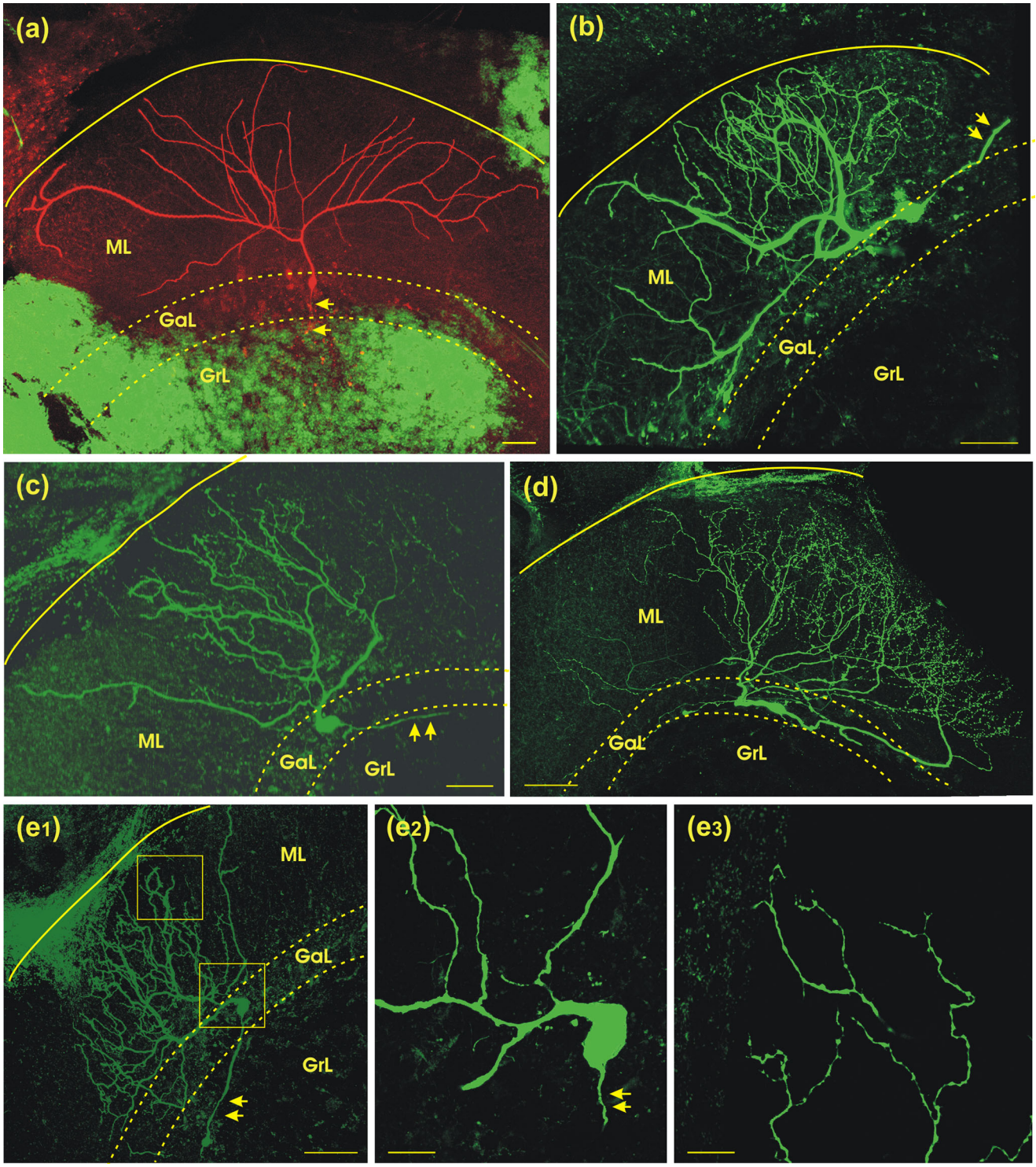

FIGURE 14 Morphology of eurydendroid cells in sagittal slices. Their soma are all located in the GaL, while their dendritic trees radiate extensively across the entire ML (a–e). (a) Example of a eurydendroid cell from a wildtype fish. Its axon projects deeply into the GrL where it was cut (arrows). (b–e) Examples of eurydendroid cells from the olig2 line. Their somas are located in the GaL, while, if labeled, their dendritic arbors radiate through the ML and their axons project along the GaL (arrows) (b, c, and e). All dendritic arbors are smooth, as shown in e2 and e3. Note that in some cases, they reach the top surface of the tissue; then turn back and branch further (d). Also note that although e2 and e3 are expensions of e1, they are 1 μm optical slices taken from the 50 μm stack of images in e1. Scale bar = 50 μm in a, b and c; 40 μm in d, 50 μm in e1, 15 μm in e2 and 10 μm in e3.

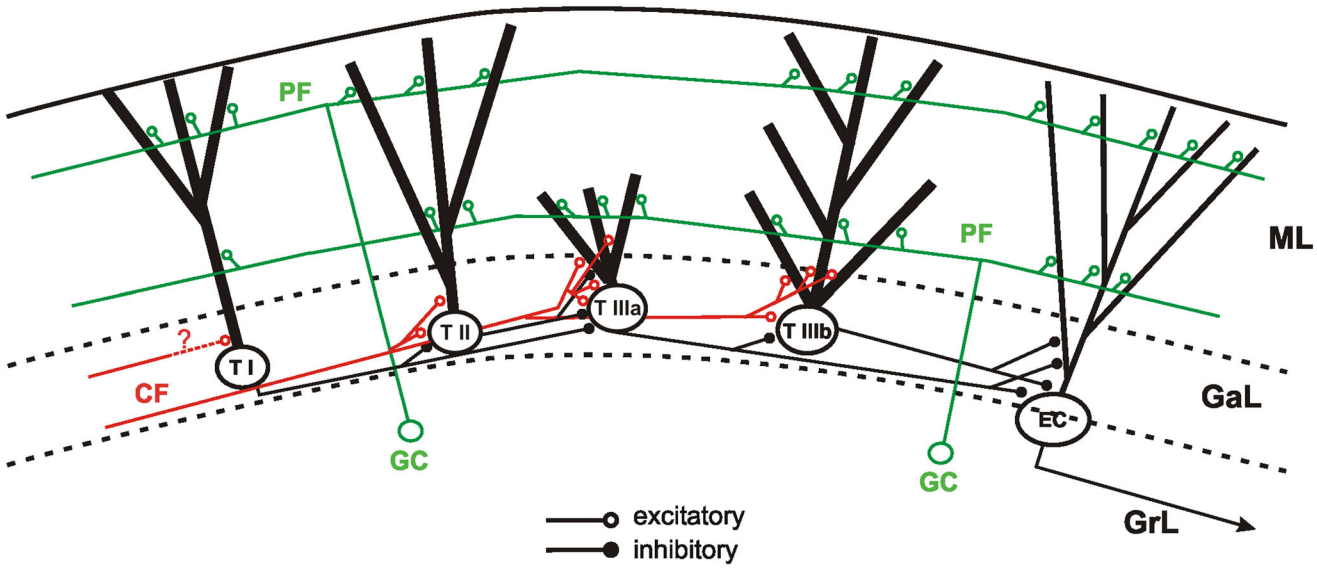

FIGURE 15 Simplified summary of our results characterizing the local circuitry of the adult zebrafish cerebellum. Schematic illustration of Purkinje cell subtypes and a single eurydendroid cell emphasizing their selective access to CF and PF stimulation. CF, climbing fiber; EC, eurydendroid cell; GaL, ganglionic layer; GC, granule cell; GrL, granular layer; ML, molecular layer; PF, parallel fiber.

these cells fire spontaneously or in response to current injection under current-clamp conditions.

It is generally agreed that axonic spikes are initiated at the axon initial segment by depolarizing Na^+ current and are responsible for transmitter release at the axon terminals (Katz, 1971; Stuart & Hausser, 1994; Zhang et al., 2012). Dendritic spikes, however, are mediated by Ca^{2+} or a mixture of both Ca^{2+} and Na^+, as specifically shown here for zebrafish Purkinje cells. Unlike axonic spikes, dendritic spikes backpropagate and are a source of additional Ca^{2+} affecting a variety of cellular functions, including synaptic plasticity (Eliers et al., 1996; Kitamura & Hausser, 2011; Zhang et al., 2012). An elegant study (Mathy et al., 2009) has shown that the duration, not the amplitude of the somatic spike is conveyed through the axon, leading to a presynaptic spike-duration-dependent release of neurotransmitter (see below for further discussion). These results suggest that our physiological subtypes may correlate with a varying impact of these subtypes on their targets (Yang & Lisberger, 2014).

4.2 | Proximity of Purkinje cells and their target eurydendroid cells

Morphological studies have shown that the adult zebrafish cerebellum consists mainly of a large, centrally positioned central lobe and a pair of small valvular ridges, all of which have a laminar structure (Bae et al., 2009; Kani, et al., 2010; Kaslin et al., 2013), similar to what has been observed for the lobules of the mammalian cerebellum (Ito, 1984). However, one of the significant anatomical variations for the cerebellum of zebrafish and other teleosts is the absence of DCN (Finger, 1978; Heap et al., 2013; Ikenaga et al., 2005), a major target of Purkinje cells axons in mammals (Ito, 1984; Meek, 1998). Instead, zebrafish eurydendroid cells (otherwise known as efferent cells or projection neurons) are intermingled with Purkinje cells in the GaL. Thus, zebrafish Purkinje cell axons project locally onto these eurydendroid cells as well as nearby Purkinje cells. This has been confirmed in the mormyrid (Zhang et al., 2012) and zebrafish (Chang et al., 2020) cerebellum. The proximity of Purkinje cells and their target cells is useful for experimentally examining how Purkinje cells influence their target cells (Matsui et al., 2014), which is nearly impossible in mammals (McDevitt, et al., 1987; but see use of dynamic clamping in Person and Raman (2011) and, to this day, leaves a significant gap in our knowledge about the cerebellar functional circuitry.

Zebrafish Purkinje cells and eurydendroid cells similarly receive PF inputs across their dendritic arbors. Eurydendroid cell responses to these PF inputs are graded, show PPF, and are sensitive to both AMPA and NMDA glutamate receptor blockers (Figure 13c), as has been shown for the analogous DCN cells in mammals (Anchisi et al., 2001) and for eurydendroid cells in the mormyrid cerebellum (Shi et al., 2008; Zhang et al., 2011). As with eurydendroid cells, responses of Purkinje cells to PF input are graded and paired-pulse facilitated, but they differ in being sensitive only to AMPA receptor blocker (Figure 10c), similar to what has been shown for Purkinje cells in both mammals (Konnerth et al., 1990; Perkel et al., 1990) and the mormyrid (Han & Bell, 2003; Zhang et al., 2011). The responses of Purkinje cells to their single CF input are all-or-none, show paired-pulse depression, and are sensitive only to AMPA glutamate receptor blocker. Although this CF response, too, is similar to that found in mammals, the waveform reported here for zebrafish is not typically complex-like, but instead may contain variable components (Figures 11b and c). Despite persistent efforts, we never recorded any all-or-none responses in the zebrafish eurydendroid cells, suggesting that they lack any CF input.

The intermingling of Purkinje cells and eurydendroid cells in zebrafish and other teleosts (Ikenaga et al., 2006) is unlikely to be the cerebellar architecture from which the spatial separation of Purkinje

cells from their DCN targets found in mammals evolved. Rather, DCN are characteristic of the lobe-finned fish, the other phylogenetic branch of the bony fish with descendants that include amniotes and amphibia. Since, so far as it is known, DCN are absent from ray-finned fish, it is likely that the arrangement of Purkinje cells and eurydendroid cells intermingled in the GaL evolved separately within this lineage. Also favoring these two cerebellar architectures evolving in separate clades is the presence of DCN in cartilagenous fish such as the elasmobranchii (sharks and rays); jawed vertebrates that developed separately from both lobe-finned and ray-finned fish (Pose-Méndez et al., 2017).

It is intriguing that two nonteleostean ray-finned fish have been found to have cerebellar efferent systems intermediate in structure between those of the DCN-lacking teleosts and species with DCN that have descended from lobe-finned and cartilaginous fish. *Polypterus senegalus*, a basal ray-finned fish, lacks DCN but has efferent cells localized in the granular layer rather than intermingled with the Purkinje cells that synapse on them in the GaL. These efferent cells do not have dendrites projecting to the ML and hence may not receive PF input (Ikenaga et al., 2021). The chondrostean *Acipenser baeri* (closely related to the sturgeons and paddlefishes) also has efferent cells in the granular layer that lack ascending dendrites (Huesa et al., 2003).

4.3 | The CF does not climb

Another difference between the zebrafish and mammalian cerebellum lies in the terminal pattern of their CFs. In mammals, the single CF branches repeatedly, climbing along the major dendrites and distal dendritic arbors throughout the entire ML, hence its name, and forming perhaps the strongest synaptic connection between a single axon and its target cell (Eccles, 1967; Ito, 1984), rivalled only by the calyx of Held in the auditory brainstem (Rodriguez-Contreras et al., 2008). The powerful CF inputs drive adaptive modification of motor gain and timing by instructing synaptic plasticity at the PF synapses (Ohtsuki et al., 2009; Welsh et al., 1995; Zang & De Schutter, 2019). It has been suggested that in zebrafish, however, the CF does not climb. Instead, its terminals are largely restricted to the GaL (Takeuchi et al., 2015), similar to what has been shown in the mormyrid cerebellum (Han et al., 2006). Using electron microscopy, Meek & Nieuwenhuyse (1991) found that a single CF can make up to 130 synapses on the soma and proximal dendrite of one mormyrid Purkinje cell (Meek & Nieuwenhuys, 1991). In frogs, which have a similar morphology of CF projections, the number of such synapses onto Purkinje cells is up to 300 (Llinas et al., 1969). This number is unknown for the zebrafish as well as for mammals where it is expected to be significantly higher due to their Purkinje cells' stereotyped climbing pattern of CFs. Although lacking this widespread presence of excitatory CF synapses throughout their dendritic arbors, at least some zebrafish Purkinje cells respond nonetheless to CF stimulation in an all-or-none and complex-like fashion at the adult (Figure 11) and larval stages (Harmon et al., 2017). This limited "climb" of CFs is another core feature of the zebrafish cerebellar module, indicating a variation in signal integration by its Purkinje cells (Zang & De Schutter, 2019).

4.4 | Functional integration of PF and CF inputs

In mammalian Purkinje cells, the narrow Na^+ spike is initiated at the axon initial segment, and then propagates along the axon to trigger neurotransmitter release at the axon terminals (Foust et al., 2010). The typically broad Ca^{2+} spike is, on the other hand, initiated throughout the dendritic arborization, reflecting the widespread proliferation of synapses of the vine-like CF. The Ca^{2+} influx generated by this spike is a major source of Ca^{2+}-dependent activity in postsynaptic dendritic spines, interacting globally with the local and more transient effects of Ca^{2+} fluxes induced by stimulated PF synapses (Eilers et al., 1996; Ohtsuki et al., 2009; Zang & De Shutter, 2019). The spatial separation of the CF and PF synapses in the mormyrid and zebrafish cerebellum, however, suggests that interactions between these two inputs may not be as robust as in mammals.

In the mammalian cerebellum, the Ca^{2+} spike is typically recorded from Purkinje cell dendrites (Llinas & Sugimori, 1980a, 1980b). In zebrafish and the mormyrid, however, as reported here and in our previous work (Han & Bell, 2003), broad and very broad spikes are mediated by both Na^+ and Ca^{2+}, but recorded from the soma. Although, in the cerebellum of teleost fish, the regions occupied by CF and PF synapses are spatially separated, we hypothesize that since CF input can still reach the soma and proximal dendrites of its Purkinje cell, it can there recruit "somatic" broad and/or very broad Ca^{2+} spikes. These spikes would then backpropagate throughout the dendritic arbor and interact with activity at multiple, concurrently stimulated PF synapses. Thus, the somatic Ca^{2+} spike would then act as a mediator, bridging the two types of input signals through a functional interaction (Ohtsuki et al., 2009; Stuart & Spruston, 2015). In other words, the neuroanatomical "disadvantage" of the spatial separation of CF and PF terminals in the zebrafish and mormyrid cerebellum could be overcome by the physiological "advantage" of backpropagated somatic Ca^{2+} spikes. This would create the similar combination of a large increase in the intracellular Ca^{2+} concentration with the local initiation of second-messenger cascades at stimulated PF synapses that is associated with PF-Purkinje cell plasticity in mammals, a hypothesis supported by our previous work demonstrating that pairing PFs and CF inputs can indeed induce PF-LTP and -LTD in mormyrid Purkinje cells (Zhang et al., 2018). It would be interesting to determine if the same is also true for the zebrafish cerebellum.

As discussed above, the signature responses of mammalian Purkinje cells to CF inputs is an all-or-none complex spike, which is usually attributed to the special pattern of synaptic contacts between a single CF and its postsynaptic Purkinje cell (Meek & Nieuwenhuys, 1991; Ohtsuki et al., 2009; Sugihara et al., 2009). Surprisingly, mechanisms underlying this unique physiological response have not been fully identified experimentally. CFs are axons of neurons in nuclei of the contralateral inferior olive. In mammals (Turecek et al., 2014) and in nonhuman primates (Welsh et al., 2011), clusters of these inferior olive neurons interconnected by gap junctions typically show a synchronous ~10 mV oscillation in their membrane potentials and, under resting conditions, fire corresponding broad (~10 ms) Ca^{2+} spikes at the peaks of this oscillation. But precisely how these broad spikes of

inferior olive neurons contribute to Purkinje cell complex spikes remains unclear.

Using dual whole-cell patch recordings in a mouse slice preparation, Mathy et al. (2009) found that the broad spikes recorded in the soma of an inferior olive neuron are conveyed to the axon as groups of action potentials or as bursting, where the number of these axonal spikes per somatic action potential varies with the phase of the cell's subthreshold oscillations. It is these groups of axonal spikes that constitute the input conveyed to a Purkinje cell by its CF. Hence, the width of the somatic broad spike, not its amplitude, in inferior olive cells determines the number of axonal spikes transmitted by the CF, where their overall duration modulates the width of the Purkinje cell complex spike. These results indicate that the intrinsic properties of inferior olive cells do affect neurotransmitter release at their axon terminals and consequently affect the response of target Purkinje cells to CF input.

Questions remain as to the relationship between pre- and postsynaptic factors at CF-Purkinje cell synapses, since the intrinsic properties of inferior olive cells and the abundant synaptic contacts made by a single CF both appear to contribute to the unique all-or-none complex spike. This is especially critical in adult zebrafish cerebellum because of the diverse morphology and physiology of its Purkinje cells. For instance, a Type I Purkinje cells has only one primary dendrite that extends past the GaL into the lower part of the ML. Consequently, its chance of receiving CF input is the lowest of these Purkinje cell types. In addition, these cells fire only narrow spikes. Thus, for Type I cells, interactions between PF and CF inputs are minimal or nonexistent, as supported by our never having recorded all-or-none CF responses, spontaneous or stimulated, from this cell type. Types III cells have multiple dendritic arbors proliferating throughout the GaL where their CFs terminate. These cells fire broad and very broad Ca^{2+} spikes. Their all-or-none CF responses can also be easily identified, suggesting strong interactions of their PF and CF inputs. Similarly, Type II cells have one or multiple dendritic arbors located in the lower molecular/ganglionic region. These cells fire a broad Ca^{2+} spike, while all-or-none CF responses have been identified in multiple cases, suggesting a significant interaction of their PF and CF inputs.

4.5 | Eurydendroid cells

Zebrafish Purkinje cells not projecting to the VN have axons that terminate locally on eurydendroid cells that are the functional equivalent of mammalian DCN cells, significantly so in that both transmit cerebellar output to many other regions of the brain (Heap et al., 2013). As an integral part of the cerebellar module, this cell type has been extensively investigated in the mammalian cerebellum (Anchisi et al., 2001; Han et al., 2014; Ohyama et al., 2006; Uusisaari & De Schutter, 2011), but less so in zebrafish larvae and minimally in the adult fish. Using the "blind-patch" procedure in wildtype fish, we have shown that zebrafish eurydendroid cells can be easily distinguished from Purkinje cells based on their morphology, pharmacology and physiology; in particular, we recorded narrow overshoot Na^+ spikes only from eurydendroid cells. However, recording from eurydendroid cells in wildtype fish was challenging to us because of a low probability for accessing them by patching cells at random (<10%).

To compensate for this, we also used a preparation of a transgenetic zebrafish line for which the transcription factor *olig2* is expressed in a set of glutamatergic eurydendroid cells (Bae et al, 2009; McFarland et al, 2008; Kani et al., 2010, Matsui et al., 2014). Fluorescent-labeled *olig2* cells were easily identified and selected for patch recording and demonstrated physiological and pharmacological properties that were similar to those of our blind-patched eurydendroid cells. Larval-stage *olig2* cells integrate both inhibitory and excitatory inputs and have been shown to be involved in fictive swimming (Harmon et al., 2020). In the line with these investigations, our recordings also show that both glutamatergic *olig2* and the non-*olig2* eurydendroid cells are present in the adult zebrafish cerebellum, and are characterized by physiological and pharmacological properties similar to those reported for mammalian DCN cells (Anchisi et al., 2001; Han et al., 2014) and mormyrid eurydendroid cells (Han & Bell, 2003; Shi et al., 2008; Zhang et al., 2011). Interestingly, the IPSC size in eurydendroid cells depends on the presynaptic spike duration rather than on its amplitude (Harmon et al., 2020), suggesting that the broad and very broad spikes fired by zebrafish Purkinje cells may affect their target cells differently, particularly in terms of inhibitory strength.

Morphologically, eurydendroid cells are located in the GaL or directly beneath it. Their dendritic arbors are smooth and oriented in the sagittal plane and extend across the entire ML. They appear flattened, although to a much less extent than the corresponding cells of the mormyrid (Han et al., 2006; Nieuwenhuys & Nicholson, 1969). As we have also seen in the mormyrid, zebrafish eurydendroid cell axons, if not cut in the slice preparation, can be traced for more than 100 μm in some cases, without collaterals or terminals.

4.6 | Comparing zebrafish cerebellum with those of the mormyrid and mammals

Despite decades of research and the establishment of a stereotyped modular organization among the cerebellum of vertebrates (Cerminara, et al., 2015; Kalueff et al., 2014; Friedrich et al., 2010; Ruigrok, 2011; Voogd & Glickstein, 1998), numerous remaining challenges have led to particular interest in smaller cerebellum and their roles in nervous systems that are more accessible for investigation. While zebrafish larvae have gathered much attention in the past decade as a focus for the study of cerebellar function (Fetcho, 2012; Okamoto, 2014), the mormyrid cerebellum also remains a useful alternative as a model system because of it characteristic morphological features (Nieuwenhuys & Nicholson, 1969; Bell & Szabo, 1986) and its involvement in fish's electrosensory system (Bell et al., 1992; Russell & Bell, 1978; Alviña & Sawtell, 2014).

As discussed earlier, the cerebellum of zebrafish and other teleost fish share many core features with those of mammals. However, there are two significant differences. One is the proximity of Purkinje cells and their target cells, for example, the eurydendroid cells and

neighboring Purkinje cells in teleosts. In mammals, Purkinje cells also inhibit neighboring Purkinje cells and ML interneurons via axon collaterals (Oldfield et al., 2010; Orduz & Liano, 2007; Sugihara et al., 2009; Witter et al., 2016), but the major projections of their axons travel long distance to reach target cells in the DCN or VN in the brainstem (Sugihara & Shinoda, 2007). It is feasible to assume that these two pathways serve different functions in mammals. As teleosts lack DCN, their functionally homologous eurydendroid cells are intermingled with the Purkinje cells that project to them (Finger, 1978; Meek, 1998). Although this provides a unique opportunity for characterizing how a single Purkinje cell controls its target cells (Zhang et al., 2012; Chang et al., 2020), the functional significance of these two anatomically similar projections remains to be investigated.

Another major difference from mammals found in the teleost cerebellum is the spatial separation of territories for PF and CF synapses in Purkinje cells. For mammals, the intermingling of the two inputs throughout the dendritic arbor (Sugihara et al., 2009), and the resulting interaction of their signals is the basis of a fundamental mechanism for motor learning (Johansson et al., 2014; Schmolesky et al., 2002; Thompson & Steinmetz, 2009). In teleosts (or at least in so far as has been investigated in zebrafish and the mormyrid), PF and CF terminals are spatially separated. For the mormyrid, experimental evidence indicates that the different inputs from these sources can interact, and that the PF-Purkinje cell plasticity believed to underlie many conditioning mechanisms also occurs (Bell et al., 2008; Zhang et al., 2018). The question remains as to how these neuronal signals from a Purkinje cell's PFs and single CF interact with one another in zebrafish. As discussed earlier, the answer appears to be that the broad Ca^{2+} spikes, which can be recorded in the Purkinje cell soma in zebrafish and the mormyrid, but not in mammals, are likely to have been recruited by CF input. Nevertheless, the hypothesis of interaction of PF and CF signals in zebrafish Purkinje cells remain to be tested, especially considering of diversity of Purkinje cell physiology, morphology, and consequentially their potential selectivity of PF and CF inputs.

5 | CONCLUSIONS

The larval zebrafish cerebellum is an attractive candidate for study due to its small size and accessibility to population imaging, visualized electrophysiological recordings, and cell-type specific genetic manipulations of its neural activity. Much has been gained from this model in terms of our knowledge of how simplified systems coordinate sensory input with behavior through cerebellum-dependent transformations. In line with the results of another recent investigation (Chang et al., 2020), our study in adult zebrafish shows, however, that the modular organization of its cerebellum cannot be assumed to be uniform. The diversified dendritic arbors of its Purkinje cells allow them to receive PF and CF inputs selectively, and the variable intrinsic properties of its PC subtypes suggest that the corresponding integration of PF and CF signals is likely to be cell-type specific. Thus, the functional circuitry of the adult zebrafish cerebellum is remarkably different from that established in mammals, and the neural computations or learning rules established in larval fish remain to be updated for a full understanding of the adult fish cerebellum.

ACKNOWLEDGMENTS

The authors thank Dr. Zhigang Shi for help with the statistical analysis, and Drs. David Perkel, Eric Lumsden, Katie Stanchak, Kimberly Miller, and John Welsh for many helpful discussions and for their valuable comments on the manuscript. This work was supported by grant from the National Science Foundation (IOS 1929489 to V. Z. H.) and by REP program from Seattle Children's Research Institute (to V. Z. H.), and grant from National Natural Science Foundation of China (to Y. Z.).

CONFLICT OF INTEREST

The authors declare no conflict of interest.

DATA AVAILABILITY STATEMENT

The data that support the findings of this study are available from the corresponding author upon reasonable request.

ORCID

Victor Z. Han https://orcid.org/0000-0003-2298-4859

PEER REVIEW

The peer review history for this article is available at https://publons.com/publon/10.1002/cne.25435.

REFERENCES

Ahrens, M. B., Li, J. M., Orger, M. B., Robson, D. N., Schier, A. F., Engert, F., & Portugues, R. (2012). Brain-wide neuronal dynamics during motor adaptation in zebrafish. *Nature*, *485*(7399), 471–477.

Ahrens, M. B., Orger, M. B., Robson, D. N., Li, J. M., & Keller, P. J. (2013). Whole-brain functional imaging at cellular resolution using light-sheet microscopy. *Nature Methods*, *10*, 413–420.

Aizenberg, M., & Schuman, E. M. (2011). Cerebellar-dependent learning in larval zebrafish. *Journal of Neuroscience*, *31*(24), 8708–8712.

Alviña, K., & Sawtell, N. B. (2014). Sensory processing and corollary discharge effects in posterior caudal lobe Purkinje cells in a weakly electric mormyrid fish. *Journal of Neurophysiology*, *112*(2), 328–339.

Anchisi, D., Scelfo, B., & Tempia, F. (2001). Postsynaptic currents in deep cerebellar nuclei. *Journal of Neurophysiology*, *85*(1), 323–331.

Azevedo, F. A. A., Carvalho, L. R., Grinberg, L. T., Farfel, J. M., Ferretti, R. E., Leite, R. E., Filho, W. J., Lent, R., & Herculano-Houzel, S. (2009). Equal numbers of neuronal and nonneuronal cells make the human brain an isometrically scaled-up primate brain. *Journal of Comparative Neurology*, *513*(5), 532–541.

Bae, Y. K., Kani, S., Shimizu, T., Tanabe, K., Nojima, H., Kimura, Y., Higashijima, S., & Hibi, M. (2009). Anatomy of zebrafish cerebellum and screen for mutations affecting its development. *Developmental Biology*, *330*(2), 406–426.

Bell, C. C., Grant, K., & Serrier, J. (1992). Sensory processing and corollary discharge effects in the mormyromast regions of the mormyrid electrosensory lobe. I. Field potentials, cellular activity in associated structures. *Journal of Neurophysiology*, *68*, 843–858.

Bell, C. C., & Szabo, T. (1986). Electroreception in mormyrid fish: Central anatomy. In: T. H. Bullock, & W. Heiligenberg (eds.): *Electroreception*. New York: John Wiley & Sons. pp. 375–421.

Bell, C. C., Han, V. Z., & Sawtell, N. B. (2008). Cerebellum-like structures and their implications for cerebellar function. *Annual Review Neuroscience*, *31*, 1–24.

Blank, M., Guerim, L. D., Cordeiro, R. F., & Vianna, M. R. (2009). A one-trial inhibitory avoidance task to zebrafish: Rapid acquisition of an NMDA-dependent long-term memory. *Neurobiology of Learning and Memory*, *92*(4), 529–534.

Buckner, R. L. (2013). The cerebellum and cognitive function: 25 years of insight from anatomy and neuroimaging. *Neuron*, *80*(3), 807–815.

Cerminara, N. L., & Apps, R. (2011). Behavioral significance of cerebellar modules. *Cerebellum*, *10*(3), 484–494.

Cerminara, N. L., Lang, E. J., Sillitoe, R. V., & Apps, R. (2015). Redefining the cerebellar cortex as an assembly of non-uniform Purkinje cell microcircuits. *Nature Review Neuroscience*, *16*(2), 79–93.

Chang, W., Pedroni, A., Hohendorf, V., Giacomello, S., Hibi, M., Köster, R. W., & Ampatzis, K. (2020). Functionally distinct Purkinje cell types show temporal precision in encoding locomotion. *Proceedings of the National Academy Sciences of the United States of America*, *117*(29), 17330–17337.

Chang, W., Pedroni, A., Köster, R. W., Giacomello, S., & Ampatzis, K. (2021). Purkinje cells located in the adult zebrafish valvula cerebelli exhibit variable functional responses. *Scientific Reports*, *11*(1), 18408.

Dohaku, R., Yamaguchi, M., Yamamoto, N., Shimizu, T., Osakada, F., & Hibi, M. (2019). Tracing of afferent connections in the zebrafish cerebellum using recombinant rabies virus. *Frontiers in Neural Circuits*, *13*, 30.

Dow, R. S., & Moruzzi, G. (1958). *The physiology and pathology of the cerebellum*. Minneapolis, University of Minnesota, p580.

Eccles, J. C. (1967). Circuits in the cerebellar control of movement. *Proceedings of the National Academy Sciences of the United States of America*, *58*(1), 336–343.

Eilers, J., Plant, T., & Konnerth, A. (1996). Localized calcium signaling and neuronal integration in cerebellar Purkinje neurons. *Cell Calcium*, *20*(2), 215–226.

Fetcho, J. R. (2012). Neuroscience: Crystal-clear brains. *Nature*, *485*(7389), 453–454.

Finger, T. E. (1978). Efferent neurons of the teleost cerebellum. *Brain Research*, *153*, 608–614.

Finger, T. E. (1983). Organization of the teleost cerebellum. In: Northcutt, R. G., Davis, R. E., (eds.) *Fish Neurobiology*, (Vol. 1, pp. 261–284). Ann Arbor: University of Michigan Press.

Foust, A., Popovic, M., Zecevic, D., & McCormick, D. A. (2010). Action potentials initiate in the axon initial segment and propagate through axon collaterals reliably in cerebellar Purkinje neurons. *Journal of Neuroscience*, *30*(20), 6891–6902.

Friedrich, R. W., Jacobson, G. A., & Zhu, G. (2010). Circuit neuroscience in zebrafish. *Current Biology*, *20*(8), R371–R381.

Gilbert, P. F., & Thach, W. T. (1977). Purkinje cell activity during motor learning. *Brain Research*, *128*(2), 309–328.

Hamling, K. R., Tobias, Z. J., & Weissman, T. A. (2015). Mapping the development of cerebellar Purkinje cells in zebrafish. *Developmental Neurobiology*, *75*, 1174–1188.

Han, V. Z., & Bell, C. C. (2003). Physiology of cells in the central lobes of the mormyrid cerebellum. *Journal of Neuroscience*, *23*, 11147–11157.

Han, V. Z., Meek, J., Campbell, H. R., & Bell, C. C. (2006). Cell morphology and circuitry in the central lobes of the mormyrid cerebellum. *Journal of Comparative Neurology*, *497*, 309–325.

Han, V. Z., Magnus, G., Zhang, Y., Wei, A. D., & Turner, E. (2014). Bidirectional modulation of deep cerebellar nuclear cells revealed by optogenetic manipulation of inhibitory inputs from Purkinje cells. *Neuroscience*, *277*, 250–266.

Han, V. Z., & Welsh, J. P. (2014). Diversity of Purkinje cell morphology and physiology in the cerebellum of the adult zebrafish (Abstract). *Society for Neuroscience*, 540.01/MM8.

Harmon, T. C., Magaram, U., McLean, D. L., & Raman, I. M. (2017). Distinct responses of Purkinje neurons and roles of simple spikes during associative motor learning in larval zebrafish. *eLife*, *6*, e22537.

Harmon, T. C., McLean, D. L., & Raman, I. M. (2020). Integration of swimming-related synaptic excitation and inhibition by olig2^{+}eurydendroid neurons in larval zebrafish cerebellum. *Journal of Neuroscience*, *40*, 3063–3074.

Hawkes, R., & Herrup, K. (1995). Aldolase C/zebrin II and the regionalization of the cerebellum. *Journal of Molecular Neuroscience*, *6*(3), 147–158.

Heap, L. A., Goh, C. C., Kassahn, K. S., & Scott, E. K. (2013). Cerebellar output in zebrafish: An analysis of spatial patterns and topography in eurydendroid cell projections. *Frontiers in Neural Circuits*, *7*, 53.

Herculano-Houzel, S. (2009). The human brain in numbers: A linearly scaled-up primate brain. *Frontiers in Human Neuroscience*, *3*, 31.

Herrup, K., & Trenkner, E. (1987). Regional differences in cytoarchitecture of the weaver cerebellum suggest a new model for weaver gene action. *Neuroscience*, *23*(3), 871–885.

Hibi, M., Matsuda, K., Takeuchi, M., Shimizu, T., & Murakami, Y. (2017). Evolutionary mechanisms that generate morphology and neural-circuit diversity of the cerebellum. *Development, Growth & Differentiation*, *59*(4), 228–243.

Hinz, F. I., Aizenberg, M., Tushev, G., & Schuman, E. M. (2013). Protein dynthesis-dependent associative long-term memory in larval zebrafish. *Journal of Neuroscience*, *33*(39), 15382–15387.

Hoxha, E., Tempia, F., Lippiello, P., & Miniaci, M. C. (2016). Modulation, plasticity and pathophysiology of the parallel fiber-Purkinje cell synapse. *Frontiers in Synaptic Neuroscience*, *8*, 35.

Hsieh, J. Y., Ulrich, B., Issa, F. A., Wan, J., & Papazian, D. M. (2014). Rapid development of Purkinje cell excitability, functional cerebellar circuit, and afferent sensory input to cerebellum in zebrafish. *Frontiers in Neural Circuits*, *8*, 147.

Huesa, G., Anadón, R., & Yáñez, J. (2003). Afferent and efferent connection of the cerebellum of the chondrostean *Acipenser baeri*: A carbocyanine dye (DiI) tracing study. *Journal of Comparative Neurology*, *460*(3), 327–344.

Ikenaga, T., Yoshida, M., & Uematsu, K. (2005). Morphology and immunohistochemistry of efferent neurons of the goldfish corpus cerebelli. *Journal of Comparative Neurology*, *487*(3), 300–311.

Ikenaga, T., Yoshida, M., & Uematsu, K. (2006). Cerebellar efferent neurons in teleost fish. *Cerebellum*, *5*(4), 268–274.

Ikenaga, T., Shimomai, R., Hagio, H., Kimura, S., Matsumoto, K., Kato, D. I., Uesugi, K., Takeuchi, A., Yamamoto, N., & Hibi, M. (2021). Morphological analysis of the cerebellum and its efferent system in a basal actinopterygian fish, Polypterus senegalus. *Journal of Comparative Neurology*, *530*(8), 1231–1246.

Ito, M. (1984). *The Cerebellum and Neural Control*. New York: Raven.

Ito, M. (2002). The molecular organization of cerebellar long-term depression. *Nature Review Neuroscience*, *3*(11), 896–902.

Ito, M. (2008). Control of mental activities by internal models in the cerebellum. *Nature Review Neuroscience*, *9*, 304–313.

Johansson, F., Jirenhed, D. A., Rasmussen, A., Zucca, R., & Hesslow, G. (2014). Memory trace and timing mechanism localized to cerebellar Purkinje cells. *Proceedings of the National Academy Sciences of the United States of America*, *111*(41), 14930–14934.

Kalueff, A. V., Stewart, A. M., & Gerlai, R. (2014). Zebrafish as an emerging model for studying complex brain disorders. *Trends in Pharmacological Science*, *35*(2), 63–75.

Kani, S., Bae, Y., Shimizu, T., Tanabe, K., Satou, C., Parsons, M. J., Scott, E., Higashijima, S., & Hibi, M. (2010). Proneural gene-linked neurogenesis in zebrafish cerebellum. *Developmental Biology*, *343*(1–2), 1–17.

Kaslin, J., Kroehne, V., Benato, F., Argenton, F., & Brand, M. (2013). Development and specification of cerebellar stem and progenitor cells in zebrafish: From embryo to adult. *Neural Development*, *8*, 9.

Katz, B. (1971). Quantal mechanism of neural transmitter release. *Science*, *173*(3992), 123–126.

Kitamura, K., & Häusser, M. (2011). Dendritic calcium signaling triggered by spontaneous and sensory-evoked climbing fiber input to cerebellar Purkinje cells *in vivo*. *Journal of Neuroscience*, *31*(30), 10847–10858.

Knogler, L. D., Markov, D. A., Dragomir, E. I., Štih, V., & Portugues, R. (2017). Sensorimotor representations in cerebellar granule cells in larval zebrafish are dense, spatially organized, and non-temporally patterned. *Current Biology*, *27*(9), 1288–1302.

Knogler, L. D., Andreas, M., Kist, A. M., & Portugues, R. (2019). Motor context dominates output from Purkinje cell functional regions during reflexive visuomotor behaviours. *Elife*, *8*, e42138.

Konnerth, A., Llano, I., & Armstrong, C. M. (1990). Synaptic currents in cerebellar Purkinje cells. *Proceedings of the National Academy Sciences of the United States of America*, *87*(7), 2662–2665.

Lee, K. H., Mathews, P. J., Reeves, A. M., Choe, K. Y., Jami, S. A., Serrano, R. E., & Otis, T. S. (2015). Circuit mechanisms underlying motor memory formation in the cerebellum. *Neuron*, *86*(2), 529–540.

Lin, Q., Manley, J., Helmreich, M., Schlumm, F., Li, J. M., Robson, D. N., Engert, F., Schier, A., Nöbauer, T., & Vaziri, A. (2020). Cerebellar neurodynamics predict decision timing and outcome on the single-trial. *Cell*, *180*(3), 536–551.

Linden, D. J. (2003). From molecules to memory in the cerebellum. *Science*, *301*(5640), 1682–1685.

Llinas, R., Bloedel, J. R., & Hillman, D. E. (1969). Functional characterization of neuronal circuitry of frog cerebellar cortex. *Journal of Neurophysiology*, *32*(6), 847–870.

Llinas, R., & Sugimori, M. (1980a). Electrophysiological properties of *in vitro* Purkinje cell somata in mammalian cerebellar slices. *Journal of Physiology (London)*, *305*, 171–195.

Llinas, R., & Sugimori, M. (1980b). Electrophysiological properties of *in vitro* Purkinje cell dendrites in mammalian cerebellar slices. *Journal of Physiology (London)*, *305*, 197–213.

Longair, M. H., Baker, D. A., & Armstrong, J. D. (2011). Simple Neurite Tracer: Open source software for reconstruction, visualization and analysis of neuronal processes. *Bioinformatics*, *27*(17), 2453–2454.

Marques, J. C., Li, M., Schaak, D., Robson, D. N., & Li, J. M. (2020). Internal state dynamics shape brain wide activity and foraging behaviour. *Nature*, *577*(7789), 239–243.

Mathy, A., Ho, S. S., Davie, J. T., Duguid, I. C., Clark, B. A., & Häusser, M. (2009). Encoding of oscillations by axonal bursts in inferior olive neurons. *Neuron*, *62*(3), 388–399.

Matsui, H., Namikawa, K., Babaryka, A., & Köster, R. W. (2014). Functional regionalization of the teleost cerebellum analyzed *in vivo*. *Proceedings of the National Academy Sciences of the United States of America*, *111*(32), 11846–11851.

McDevitt, C. J, Ebner, T. J., & Bloede, J. R. (1987). Relationships between simultaneously recorded Purkinje cells and nuclear neurons. *Brain Research*, *425*(1), 1–13.

McFarland, K. A., Topczewska, J. M., Weidinger, G., Dorsky, R. I., & Appel, B. (2008). Hh and Wnt signaling regulate formation of *olig2*$^{+}$ neurons in the zebrafish cerebellum. *Developmental Biology*, *318*(1), 162–171.

Meek, J. (1998). Holosteans and teleosts. In R. Nieuwenhuys, H. J. Ten Donkelaar, & C. Nicholson (Eds.), *The central nervous system of vertebrates* (pp. 759–937). Berlin: Springer.

Meek, J., & Nieuwenhuys, R. (1991). Palisade pattern of mormyrid Purkinje cells: A correlated light and electron microscopic study. *Journal of Comparative Neurology*, *306*, 156–192.

Mitoma, H., Kakei, S., Yamaguchi, K., & Manto, M. (2021). Physiology of cerebellar reserve: Redundancy and plasticity of a modular machine. *International Journal of Molecular Science*, *22*, 4777.

Nairn, J. G., Bedi, K. S., Mayhew, T. M., & Campbell, L. F. (1989). On the number of Purkinje cells in the human cerebellum: Unbiased estimates obtained by using the "fractionator". *Journal of Comparative Neurology*, *290*, 527–532.

Nieuwenhuys, R., & Nicholson, C. (1969). A survey of the general morphology, the fiber connections, and the possible functional significance of the gigantocerebellum of mormyrid fishes. In R. Llinas (Ed.), *Neurobiology of Cerebellar Evolution and Development* (pp. 107–169). Chicago: American Medical Association.

Ohtsuki, G., Piochon, C., & Hansel, C. (2009). Climbing fiber signaling and cerebellar gain control. *Frontiers in Cellular Neuroscience*, *3*, 4.

Ohyama, T., Nores, W. L., Medina, J. F., Riusech, F. A., & Mauk, M. D. (2006). Learning-induced plasticity in deep cerebellar nucleus. *Journal of Neuroscience*, *26*(49), 12656–12663.

Okamoto, H. (2014). Minicerebellum, now available for reductionists' functional study. *Proceedings of the National Academy Sciences of the United States of America*, *111*(32), 11580–11581.

Oldfield, C. S., Marty, A., & Stell, B. M. (2010). Interneurons of the cerebellar cortex toggle Purkinje cells between up and down states. *Proceedings of the National Academy Sciences of the United States of America*, *107*(29), 13153–13158.

Orduz, D., & Llano, I. (2007). Recurrent axon collaterals underlie facilitating synapses between cerebellar Purkinje cells. *Proceedings of the National Academy Sciences of the United States of America*, *104*(45), 17831–17836.

Perkel, D. J., Hestrin, S., Sah, P., & Nicoll, R. A. (1990). Excitatory synaptic currents in Purkinje cells. *Proceedings of the Royal Society Biological Science*, *241*(1301), 116–121.

Person, A., & Raman, I. (2011). Purkinje neuron synchrony elicits time-locked spiking in the cerebellar nuclei. *Nature*, *481*(7382), 502–505.

Portugues, R., Feierstein, C. E., Engert, F., & Orger, M. B. (2014). Whole-brain activity maps reveal stereotyped, distributed networks for visuomotor behavior. *Neuron*, *81*(6), 1328–1343.

Pose-Méndez, S., Rodríguez-Moldes, I., Candal, E., Mazan, S., & Anadón, R. (2017). A developmental study of the cerebellar nucleus in the catshark, a basal gnathostome. *Brain, Behavior and Evolution*, *89*, 1–14.

Rodríguez-Contreras, A., van Hoeve, J. S., & Habets, R. L. (2008). Dynamic development of the calyx of Held synapse. *Proceedings of the National Academy Sciences of the United States of America*, *105*(14), 5603–5608.

Ruigrok, T. J. (2011). Ins and outs of cerebellar modules. *Cerebellum*, *10*(3), 464–474.

Russell, C. J., & Bell, C. C. (1978). Neuronal responses to electrosensory input in mormyrid valvula cerebelli. *Journal of Neurophysiology*, *41*(6), 1495–1510.

Sarnaik, R., & Raman, I. (2018). Control of voluntary of optogenetically perturbed locomotion by spike rate and timing of neurons of the mouse cerebellar nuclei. *eLife*, *7*, 329546.

Scalise, K., Shimizu, T., Hibi, M., & Sawtell, N. B. (2016). Responses of cerebellar Purkinje cells during fictive optomotor behavior in larval zebrafish. *Journal of Neurophysiology*, *116*(5), 2067–2080.

Schindelin, J., Arganda-Carreras, I., Frise, E., Kaynig, V., Longair, M., Pietzsch, T., Preibisch, S., Rueden, C., Saalfeld, S., Schmid, B., Tinevez, J. -V., White, D. J., Hartenstein, V., Eliceiri, K., Tomancak, P., & Cardona, A. (2012). Fiji: An open-source platform for biological-image analysis. *Nature Methods*, *9*, 676–682.

Schmahmann, J. D., Guell, X., Stoodley, C. J., & Halko, M. A. (2019). The theory and neuroscience of cerebellar cognition. *Annual Review Neuroscience*, *42*, 337–364.

Schmolesky, M. T., Weber, J. T., de Zeeuw, C. I., & Hansel, C. (2002). The making of a complex spike: Ionic composition and plasticity. *Annals of the New York Academy of Sciences*, *978*, 359–390.

Sengupta, M., & Thirumalai, V. (2015). AMPA receptor mediated synaptic excitation drives state-dependent bursting in Purkinje neurons of zebrafish larvae. *eLife*, *4*, e09158.

Shi, Z., Zhang, Y., Meek, J., Qiao, J. T., & Han, V. Z. (2008). The neuronal organization of a unique cerebellar specialization: The valvula cerebelli of a mormyrid fish. *Journal of Comparative Neurology*, *509*(5), 449–473.

Stewart, A. M., Braubach, O., Spitsbergen, J., Gerlai, R., & Kalueff, A. V. (2014). Zebrafish models for translational neuroscience research: From fish tank to bedside. *Trends in Neuroscience*, *37*(5), 264–278.

Streisinger, G., & Walker, C. (1983). Induction of mutations by gamma-rays in pregonial germ cells of zebrafish embryos. *Genetics*, *103*, 125–136.

Stuart, G. J., & Hausser, M. (1994). Initiation and spread of sodium action potentials in cerebellar Purkinje cells. *Neuron*, *13*(3), 703–712.

Stuart, G. J., & Spruston, N. (2015). Dendritic integration: 60 years of progress. *Nature Neuroscience*, *18*(12), 1713–1721.

Sugihara, I., & Shinoda, Y. (2007). Molecular, topographic, and functional organization of the cerebellar nuclei: Analysis by three-dimensional mapping of the olivonuclear projection and aldolase C labeling. *Journal of Neuroscience*, *27*(36), 9696–9710.

Sugihara, I., Fujita, H., Na, J., Quy, P. N., Li, B. Y., & Ikeda, D. (2009). Projection of reconstructed single Purkinje cell axons in relation to the cortical and nuclear aldolase C compartments of the rat cerebellum. *Journal of Comparative Neurology*, *512*(2), 282–304.

Takeuchi, M., Matsuda, K., Yamaguchi, S., Asakawa, K., Miyasaka, N., Lal, P., Yoshihara, Y., Koga, A., Kawakami, K., Shimizu, T., & Hibi, M. (2015). Establishment of Gal4 transgenic zebrafish lines for analysis of development of cerebellar neural circuitry. *Developmental Biology*, *397*(1), 1–17.

Tang, T., Xiao, J., Suh, C., Burroughs, A., Cerminara, N., Jia, L., Marshall, P., Wise, A., Apps, R., Sugihara, I., & Lang, E. (2017). Heterogeneity of Purkinje cell simple spike-complex spike interactions: Zebrin- and non-zebrin-related variations. *Journal of Physiology*, *595*(15), 5341–5357.

Thompson, R. F., & Steinmetz, J. E. (2009). The role of the cerebellum in classical conditioning of discrete behavioral responses. *Neuroscience*, *162*(3), 732–755.

Turecek, J., Yuen, G. S., Han, V. Z., Zeng, X. H., Bayer, K. U., & Welsh, J. P. (2014). NMDA receptor activation strengthens weak electrical coupling in mammalian brain. *Neuron*, *81*(6), 1375–1388.

Uusisaari, M., & De Schutter, E. (2011). The mysterious microcircuitry of the cerebellar nuclei. *Journal of Physiology*, *589*(Pt. 14), 3441–3457.

Voogd, J., & Glickstein, M. (1998). The anatomy of the cerebellum. *Trends in Neuroscience*, *21*(9), 370–375.

Welsh, J. P., Lang, E. J., Sugihara, I., & Llinás, R. (1995). Dynamic organization of motor control within the olivocerebellar system. *Nature*, *374*(6521), 453–457.

Welsh, J. P., Han, V. Z., Rossic, D. J., Mohrc, C., Odagirid, M., Daunaise, J. B., & Grant, K. A. (2011). Bidirectional plasticity in the primate inferior olive induced by chronic ethanol intoxication and sustained abstinence. *Proceedings of the National Academy Sciences of the United States of America*, *108*(25), 10314–10319.

Witter, L., Rudolph, S., Pressler, R. T., Lahlaf, S. I., & Regehr, W. G. (2016). Purkinje cell collaterals enable output signals from the cerebellar cortex to feed back to Purkinje cells and interneurons. *Neuron*, *91*(2), 312–319.

Yang, Y., & Lisberger, S. G. (2014). Purkinje-cell plasticity and cerebellar motor learning are graded by complex-spike duration. *Nature*, *510*(7506), 529–532.

Zang, Y., & De Schutter, E. (2019). Climbing fibers provide graded error signals in cerebellar learning. *Frontiers In Systematic Neuroscience*, *13*, 46.

Zhang, Y., & Han, V. Z. (2007). Physiology of morphologically identified cells in the posterior caudal lobe of the mormyrid cerebellum. *Journal of Neurophysiology*, *98*(3), 1297–308.

Zhang, Y., Shi, Z., Magnus, G., Meek, J., Han, V. Z., & Qiao, J. T. (2011). Functional circuitry of a unique cerebellar specialization: The valvula cerebelli of a mormyrid fish. *Neuroscience*, *182*, 11–31.

Zhang, Y., Magnus, G., & Han, V. Z. (2012). Synaptic dynamics and long-term plasticity at synapses of Purkinje cells onto neighboring Purkinje cells of a mormyrid fish: A dual cell recording study. *Neuroscience*, *225*, 199–212.

Zhang, Y., Magnus, G., & Han, V. Z. (2018). Cell type-specific plasticity at parallel fiber synapses onto Purkinje cells in the posterior caudal lobe of the mormyrid fish cerebellum. *Journal of Neurophysiology*, *120*(2), 644–661.

How to cite this article: Magnus, G., Xing, J., Zhang, Y., & Han, V. Z. (2023). Diversity of cellular physiology and morphology of Purkinje cells in the adult zebrafish cerebellum. *Journal of Comparative Neurology*, *531*, 461–485.
https://doi.org/10.1002/cne.25435